Oxidation behaviour of PVD coated tools for metal cutting applications

Joakim Sandberg

LUND UNIVERSITY

LTH

FACULTY OF ENGINEERING

2024

MASTER THESIS
DIVISION OF PRODUCTION AND MATERIALS ENGINEERING
FACULTY OF ENGINEERING, LUND UNIVERSITY

CODEN: LUTMDN/(TMMV-5307)/1-67/2020

Author: Joakim Sandberg

Examiner: Filip Lenrick, Docent
Division of Production and Materials Engineering,
Department of Industrial and Mechanical Sciences,
Faculty of Engineering, Lund University

Supervisor: Volodymyr Bushlya, Ass. Professor
Division of Production and Materials Engineering,
Department of Industrial and Mechanical Sciences,
Faculty of Engineering, Lund University

Assistant supervisor: Rebecka Lindvall, PhD
Division of Production and Materials Engineering,
Department of Industrial and Mechanical Sciences,
Faculty of Engineering, Lund University

Company supervisors: Rachid M'Saoubi and Jon Andersson
R&D Materials and Technology Department,
Seco Tools AB, Sweden

Keywords:
Metal cutting
Machining performance
Tool wear
Wear mechanisms
Oxidation
Cemented carbide
Coating
PVD
SEM

Abstract

In the 20th century, big innovative steps were made in the cutting tool industry. Two Swedish companies, today Seco Tools AB and Sandvik Coromant, were some of the first companies to use cemented carbide as tool material. In 1969 Sandvik Coromant introduced a layer of titanium carbides on top of a cemented carbide substrate to improve its performance. Coating materials have been continuously developed since, with the aim to support the substrate of the cutting tool. Today, this means that the tool life can be extended by a factor 2 – 3 in certain applications.

Coatings are mainly deposited in either of two methods: Chemical Vapor Deposition (CVD) or Physical Vapor Deposition (PVD). High process temperatures (800 – 1000 °C for the CVD method and 400 – 600 °C for the PVD method) leads to tensile stress due to different heat expansion coefficient for the substrate and the coating material. With cathodic arc evaporation, the PVD method used for this master thesis project, compressive stress forms in the coating due to high-energy metal ions bombarding the substrate. Thin PVD coatings have beneficial properties for cutting tools used in finishing operations. Thicker CVD coatings have properties beneficial for cutting tools used in roughing operations.

This study compares the performance of four concept coatings with two reference coatings: TiN and TiAlN. The substrate material of the tool is cemented carbide, WC-6 % Co, being coated with the PVD cathodic arc technique. The coatings are heat treated in furnace as well as tested in machining operation, turning, in two different environments: argon respectively air, applied on the tool at high pressure to ensure respectively eliminate oxygen. The workpiece material to be machined was the difficult-to-cut Alloy 718, deployed both at elevated speed to stress the coating thermally for five seconds, and performance tested for a couple of minutes.

One concept coating and TiAlN showed great oxidation resistance in furnace at 800 °C, and the other coatings showed medium to low oxidation resistance. The TiAlN outperformed the other coatings in machining experiments. The as-worn tools were studied in scanning electron microscope (SEM) and X-ray energy dispersive spectroscopy (EDX) results showed insufficient data. Hence cross-sectioned tools were further investigated with SEM-EDX, which revealed distribution of elements on top of the coating after machining.

SEM studies of cross-sectioned tools used in machining revealed no oxides atop the coating. The conclusion was that the concept coatings and the TiN were not strong enough to machine Alloy 718 to reach conditions when oxidation resistance plays a sufficient role. Results showed that the coatings, with the exception of TiAlN, are most likely mechanically worn, due to adhesion of the workpiece material on the coating which removes the coating mechanically due to the movement of the adhered material. The substrate gets exposed and the contact with Alloy 718 results in its rapid wear, due to the lack of protective coating.

Acknowledgement

This master thesis is a collaboration between Seco Tools AB and the Division of Production and Materials Engineering, Department of Mechanical Engineering, Faculty of Engineering at Lund University. The tools were manufactured by Seco Tools AB in Fagersta and experiments were performed at the Division of Production and Materials Engineering in Lund.

I want to thank my industry supervisors, Rachid M'Saoubi and Jon Andersson from Seco Tools AB, for all their help and contributions to this master thesis project. I also want to thank my supervisors from the division, Volodymyr Bushlya and Rebecka Lindvall, for all the help and support. These four individuals have helped me with the project a lot, but also taught me so much and contributed to my personal development.

Other people from Seco Tools AB and the division of Production and Materials Engineering have also contributed to the project, which I also would like to express my gratitude to, a special thanks to Axel Bjerke at the division for helping with parts of the microscopy work.

Table of Contents

1. Introduction

In the 20th century, large innovative steps were made in the cutting tool industry. For example, when replacing Carbon steel with High speed steel (HSS) 1906, which made it possible to machine tougher workpiece materials, or around three times as fast. The German industrial concern Krupp commercialized the cemented carbide (CC) in 1929 and commercial production by Fagersta Bruk in 1932, today Seco Tools AB, and by Sandvikens Jernverk in 1942, today Sandvik Coromant, with the two last mentioned being international Swedish companies. Another of these big steps was in 1969 when Sandvik Coromant coated CC tools with a layer of hard carbides, and the development of coatings has played a major role in the development of modern cutting tools. [1]

With better and stronger materials being developed for use in end products, there is a constant search for even stronger and cost-efficient tools, to be able to manufacture these workpiece materials. For example, the development of jet engines basically means that the combustion temperature needs to be higher to make more efficient use of the fuel. This then means that the turbines material needs to be stable at even higher temperatures and then the cutting tools, or other manufacturing equipment needed, has to be even stronger and stay strong at high temperatures.

There are several factors to consider in a metal cutting process: the tool materials resistance against *adhesive wear, abrasive wear, diffusion* and *chemical wear.* The choice of workpiece material of course affects the characteristics of a finished product, but also has a big impact on the machinability and factors like *abrasiveness, ductility, strain hardening, thermal conductivity* and *hardness* needs to be considered. [1] Predictability of the wear and tool life is of great importance, which is why it takes a lot of research and testing before new methods and products reaches the industry.

The subject of this master thesis was brought up by the division of Production and Materials Engineering together with Seco Tools AB, as the interest of interaction between specifically designed coatings and certain workpiece materials. The oxidation effect was of interest to investigate, and how different coating materials behave in machining. The purpose of this study is to investigate possibilities of this area for future research and development.

1.1. Problem description

Is oxidation resistance an important performance factor, and to what extent, for coatings used when machining Alloy 718?

1.2. Purpose

The purpose of this master thesis project is to study the oxidation behaviour, how coatings can prevent this in metal cutting applications and which materials are suited for certain workpiece materials. Experiments needs to be designed to test these behaviours and knowledge about microscopy methods needs to be accumulated. Specific information about concept coatings is mainly for the use of Seco Tools AB and collected information might be used as base for continued research.

1.3. Scope

Workpiece material used in this project was nickel-based alloy called Alloy 718.

Tool material used in this project was cemented carbide, WC – 6 wt% (weight %) Co, with six different PVD (Physical vapor deposition) cathodic arc, monolayered, coatings. Four concept coatings will be referred to in this report as:

- C1
- C2
- C3
- C4

Which will be compared to two references coatings:

- R1: TiN
- R2: TiAlN

1.4. Limitations

Only selected coatings are subjected to the full test program and microscopy, with others being excluded after poor performance in early tests. Only C4 is performed in the last test, with it not being extensive and rather confirming the early-stage behaviour. The workpiece material was not investigated when it comes to microstructure, hardness or other details, and was relying on the given material specification.

2. Theory

This part of the report explains the theory behind this master thesis and what needs to be known to understand and help interpret the results. Therefore, it will contain some basic theory of metal cutting and why tools are worn out, what kind of wear might appear on a tool, and why coatings are used to prevent some of these. This section will explain some basics of metal cutting, wear mechanisms, workpiece material, tool material and go a bit more into specifics about coatings. In the end of the chapter, microscopy methods are briefly explained.

2.1. Metal cutting

In metal cutting, unlike shearing where there are two edges working together to divide something, there is one cutting edge removing material by forming a chip, illustrated in figure 2-1. This is the basic for many cutting processes including the two most common: turning and milling. [1]

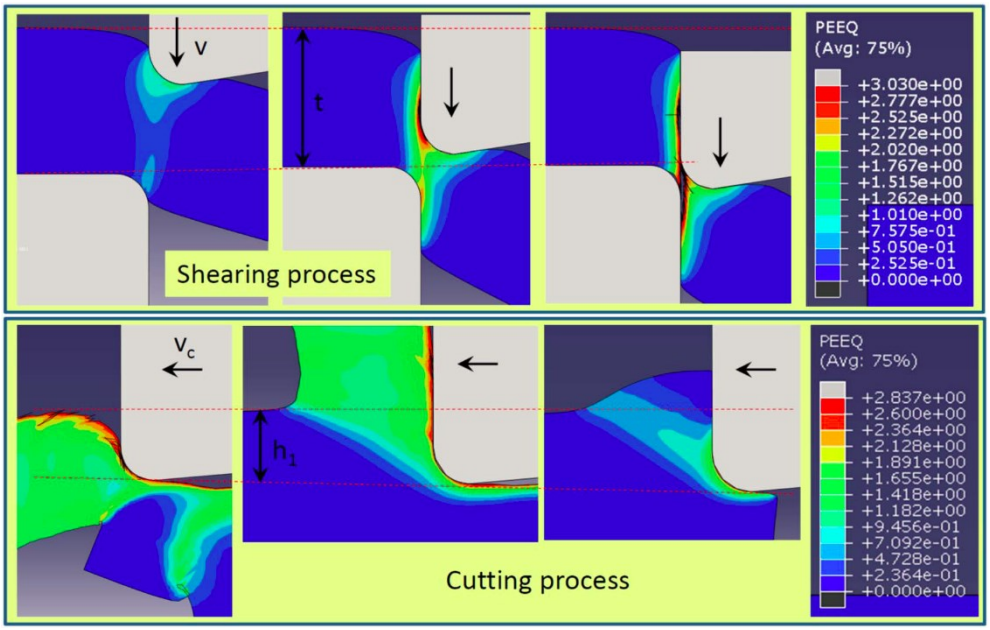

Figure 2-1 The principle of the shearing process compared to the cutting process. [1]

Cutting tool material and insert geometry has a long history and has been researched a lot. This report will not go into different shapes and geometries of cutting tools, and rather focus on the materials and reactions at the interface between tool and workpiece.

As can be seen in the simulation above, Figure 2-1, there are regions where the tension is higher, and temperatures will increase. The energy consumption of a

cutting process can be computed, if the cutting force components that act on the tool which are parallel to the cutting speed directions are identified. The cutting forces can be divided into three components, shown in Figure 2-2, which are the main cutting force, F_c, the feed force, F_f, and the passive force, F_p. Example of cutting forces in three different workpiece materials and with varying depth of cut is shown in Figure 2-3. These can be measured and the total power consumption, P_t, can be computed using Equation 2.1. [1]

$$P_t = F_c \cdot v_c + F_f \cdot v_f + F_p \cdot v_p \approx P_c = F_c \cdot v_c \qquad \textit{Equation 2.1}$$

This equation can be simplified to only involve the main cutting force and the cutting speed, since $v_f << v_c$ and $v_p << v_c$ in most cases, with the energy consumption connected to the feed is less than 1% of the total energy consumption. If the cutting resistance, Cr, is known, the main cutting force can be computed, and hence Equation 2.1 can be rewritten as Equation 2.2. [1]

$$P_c = F_c \cdot v_c = v_c \cdot h_1 \cdot b \cdot Cr \approx v_c \cdot f \cdot a_p \cdot Cr \qquad \textit{Equation 2.2}$$

Where h_1 is the theoretical cutting depth, b is the undeformed chip width, f is the feed and a_p is the depth of cut. The cutting resistance is the resistance per total chip area that the workpiece material shows in a certain application of a specific cutting tool and cutting data employed. In other words, the cutting resistance should not only be seen as a material constant, but rather a representative of material characteristics that is linked to the specific process and the microgeometry of the cutting tool. [1]

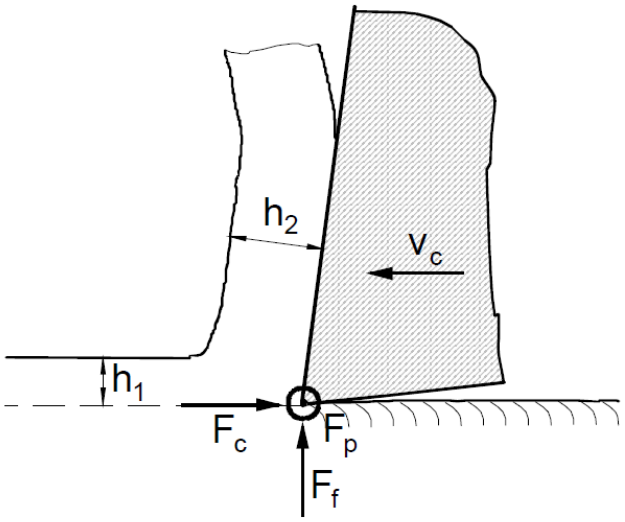

Figure 2-2 An orthogonal, 2-dimensional cutting process with the cutting forces F_c, main cutting force, F_f, feed force, and F_p, passive force, as well as the cutting speed v_c, chip velocity v_{ch} , theoretical chip thickness h_1 and real chip thickness h_2. [1]

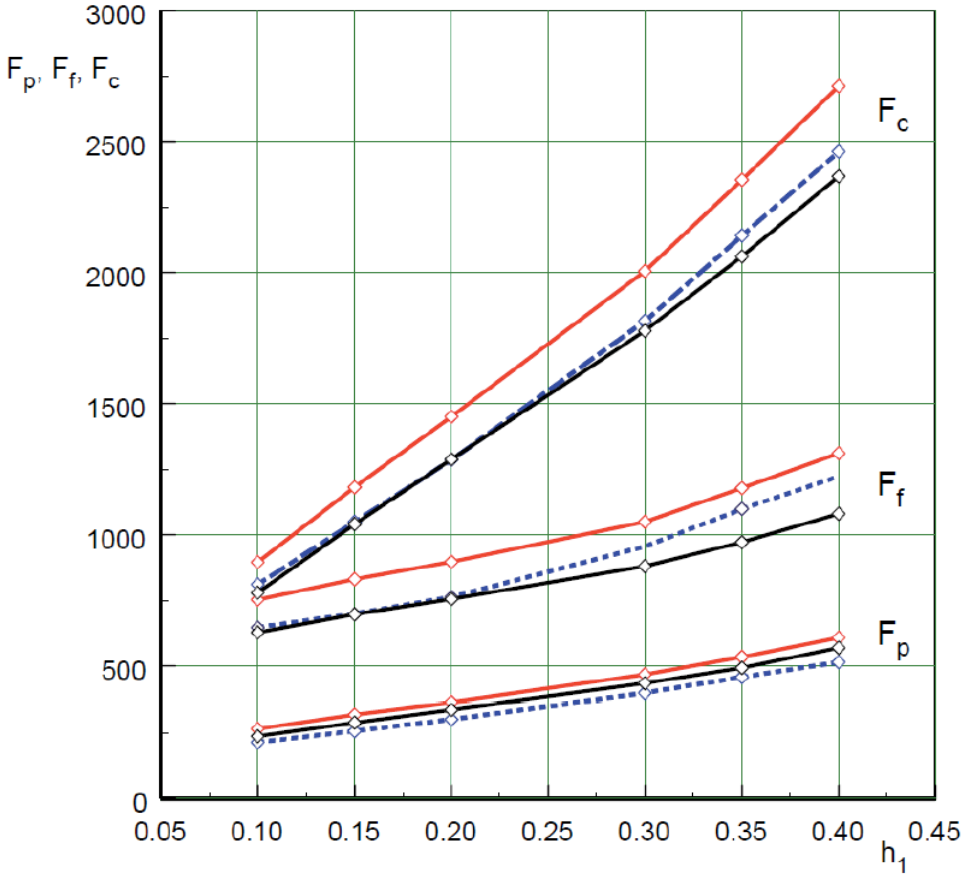

Figure 2-3 Cutting forces [N] in machining of three different workpiece materials at v_c = 240 m/min and a_p = 3 mm with different theoretical chip thickness, h_1. [2]

The total power consumption of the cutting process can be computed as the sum of the power consumption needed in each deformation zone, Equation 2.3 and illustrated in Figure 2-4. [1]

$$P_c = P_I + P_{II} + P_{III} \qquad \textit{Equation 2.3}$$

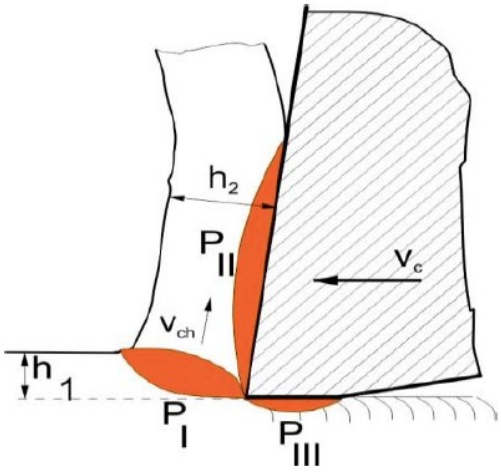

Figure 2-4 The energy the cutting process consumes in each of the three deformation zones. [1]

In the primary deformation zone, zone I, material is sheared from the workpiece and removed as a chip. In the secondary deformation zone, zone II, the chips glides across the *rake face* of the cutting tool. In the tertiary deformation zone, zone III, a new surface is generated on the workpiece and at the same time the workpiece glides towards the *clearance face*, or the *flank*, of the cutting tool. Temperature rise takes place within the space for each of the three deformation zones, which is proportional to the volume of the zone and the amount of energy converted there. With very high cutting speeds or machining workpiece material with low thermal conductivity, the process temperature can get critically high. [1]

2.1.1. Wear mechanisms and tool deterioration

Tool wear mechanisms can be divided into four physical factors, which impacts the tool by continuous loss of tool material [1]:

- *Abrasive wear*, which can occur if the workpiece material machined contains hard inclusions, will be mentioned more in section 2.1.2, and has a grinding effect on the tool.
- *Adhesive wear*, an effect where workpiece material gets micro-welded onto the cutting tool, also called *adhesion*, which causes micro-chipping of the cutting edge, seen in contact zone B in Figure 2-5.
- *Diffusion,* material transport on atomic level between the workpiece and the cutting tool. If these atomic exchanges occur, the material characteristics in those parts of the tool declines. This mechanism is strongly temperature dependent highly favourable to take place at process temperatures of 800 – 1000 ºC.
- *Chemical and electrochemical wear*, there is a chance for gases to reach the area between the tool and the chips created in a continuous cutting process, which makes it possible for oxidation to occur.

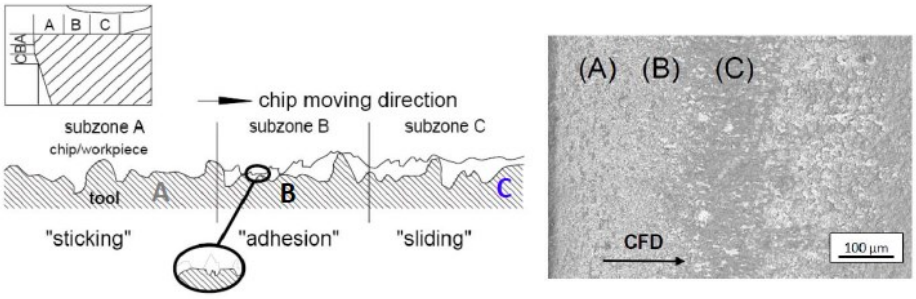

Figure 2-5 Contact area between the cutting tool and the workpiece material divided into three zones, A, B and C. [1]

Different applications and cutting tools can have different dominant mechanism affecting the tool wear, or by a combination of mechanisms. The effect of the different tool wear mechanisms depends on the process temperature, shown in Figure 2-6, with adhesive wear having big impact on the wear at lower temperatures and diffusion- and chemical wear being dominant at higher temperatures. [1]

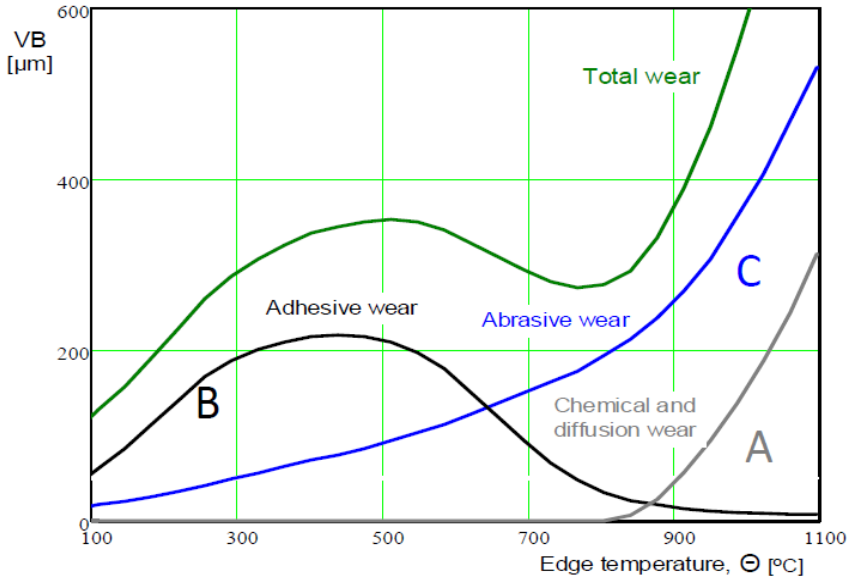

Figure 2-6 Schematic diagram of wear mechanisms on a cemented carbide cutting tool at different temperatures. [1]

Described wear mechanisms has geometrical impact on the cutting tool thorough the continual loss of tool material. These geometrical changes have impact both on the machining results and the cutting tool performance. There are three categories to describe these changes, *flank wear, crater wear* and *notch wear*, seen in Figure 2-7 from the test standard ISO 3685. [1] [3]

Flank wear means that there is a wear surface parallel to the cutting direction on the cutting tool, which leads to an increase for both the shear- and the normal forces, as well as heat generation and cutting resistance. Flank wear is often temperature-dependent, which means with bigger flank wear the wear is accelerated. As the flank is worn, the edge line position in relation to the workpiece is shifting. If this is not compensated for, the dimensions of the manufactured part get changed over time. This wear takes place in the tertiary zone, zone III above. [1]

Crater wear takes place on the rake of the cutting tool, in most cases not directly on the edge line and rather some distance from it in the chip flow direction. This wear, which experimental studies have shown, is initiated at the position of the rake where the energy consumption, and the temperature, is the highest. This primarily takes place in the secondary deformation zone, zone II above. This affects the surface contact relationship between the workpiece and the cutting tool by increasing it, which means that the shearing forces increases. This has a decisive effect on the cutting tools edge, which increase the positive rake angle and usually mean slight decrease of the cutting forces. Though as the rake wear increases, the cutting edge gets weaker and can lead to tool failure. [1]

Notch wear is primarily found on the clearance face of the tool which normally takes place where the contact between the chip and the cutting tool eases. Air with oxygen is accessible which can lead to that parts of the tools surface oxidises and easier worn off. Notch wear can also be caused by work hardening of the outer surface of the workpiece material, as well as a cast skin on the workpiece surface. [1]

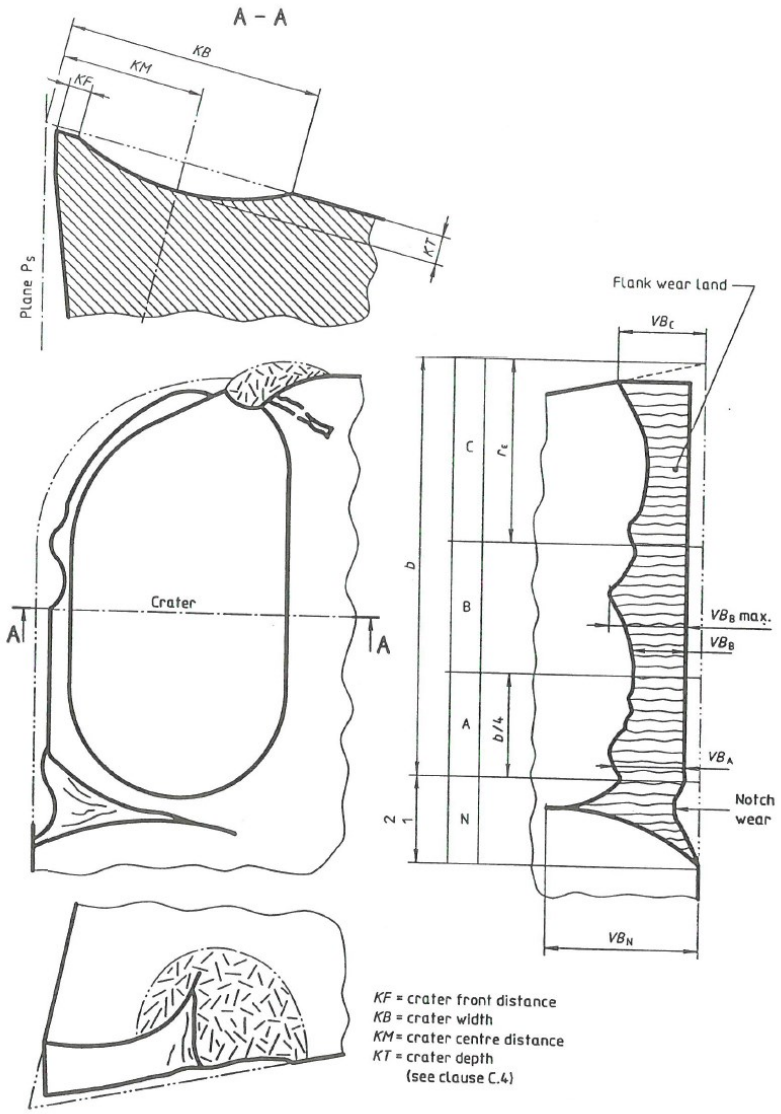

Figure 2-7 Wear types on a cutting tool in a turning application. [3]

Regarding oxidation of metals, or electrochemical reactions, that normally takes place in gaseous atmospheres, unlike corrosion of metallic materials that takes place in aqueous solutions. This is when an oxide layer or scale forms on the surface of a metal, which is sometimes termed *scaling*, *tarnishing* or *dry corrosion*. This formation is an electrochemical reaction, where metal ions are formed on the metal-scale interface when the metal atoms react with the oxygen in the atmosphere, shown with generalized reactions in Figure 2-8. The scale thickness can grow if the electrons can be conducted to the scale-gas interface, and if the metal ions can diffuse from the metal-scale interface and/or the oxygen ions can travel to the same

interface. This scale might act as a barrier with most metal oxides being highly electrically insulated, which can protect the metal from rapid oxidation. [4]

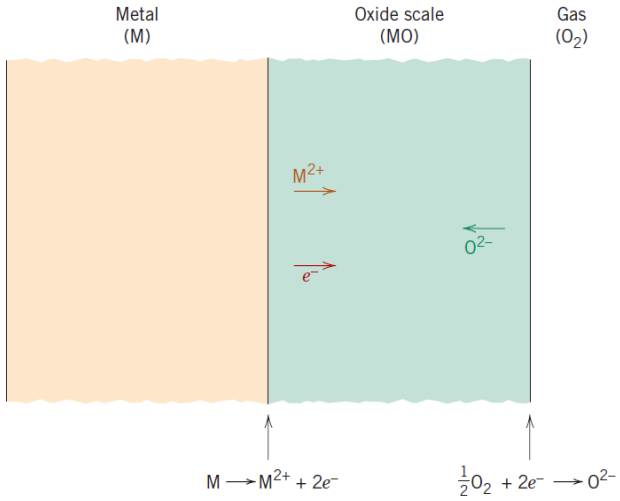

Figure 2-8 Schematic representation of the oxidation process. [4]

The rate that the reactions progress for the metal oxide scale, is one of the primary concerns for oxidation growth. This is normally measured of the weight gain per unit area, W, as a function of time. When the oxide scale adheres to the metal in a nonporous form, the growth rate is controlled by the ionic diffusion and a so-called *parabolic* weight gain is occurring, described with Equation 2.4. [4]

$$W^2 = K_1 \cdot t + K_2 \qquad \textit{Equation 2.4}$$

Where K_1 and K_2 are time-independent constants at a certain temperature. Iron, cobalt and copper are materials which follows this oxidation rate expression. For metals where the scale is porous or flakes off, the oxidation rate is expressed as *linear* growth and the weight gain can be expressed as Equation 2.5. [4]

$$W = K_3 \cdot t \qquad \textit{Equation 2.5}$$

With these circumstances, where K_3 is a constant, it means that oxygen will always be available, and the metal surface will not be protected as a reaction barrier by the oxide. Sodium, potassium and tantalum oxidation growth can be expressed as linear scale growth. *Logarithmic* oxidation is a third scale growth which forms very thin films, generally less than 100 nm, which forms at relatively low temperatures and forms as Equation 2.6. [4]

$$W = K_4 \log(K_5 \cdot t + K_6) \qquad \textit{Equation 2.6}$$

Where K_4, K_5 and K_6 are constants. Aluminium, copper and iron has shown logarithmic oxidation behaviour at near-ambient temperatures and is the most

beneficial one that can protect the metal from rapid oxidation growth and consume less material. All three oxidation rate laws are represented in Figure 2-9. [4]

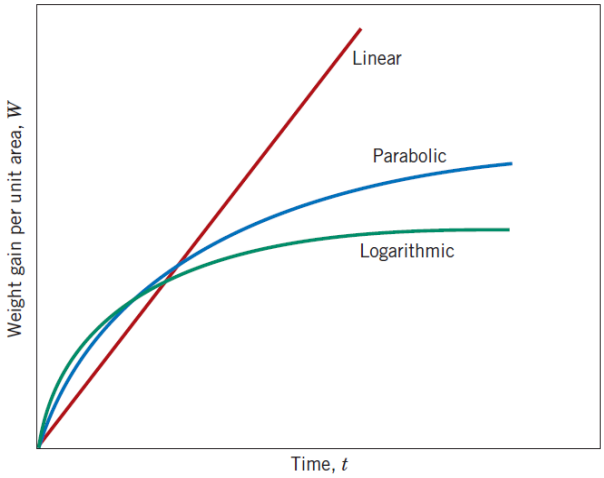

Figure 2-9 Scale growth for linear-, parabolic- and logarithmic rate laws. [4]

Bushlya et al. [5] studied the oxygen influenced tool wear, by use of a controlled environment chamber when machining with three different tool materials (cemented carbide, cermet and PCBN) in three different workpiece materials (alloyed steel, hardened tool steel and superalloy Alloy 718). All except one combination (hardened tool steel machined with PCBN) showed more intense cratering in oxidized environment. It was concluded that the flank wear is more intense when machining in an argon environment. The oxidation only occurred at higher speeds, and when machining in Alloy 718, cratering was reduced due to oxidation of workpiece material with formation of Al_2O_3 on the tool.

Greczynski et al. [6] annealed PVD coated tools in air at temperature range of 500 – 800 °C for one hour, and one sample was annealed at 600 °C for five hours, to compare the oxidation behaviour. It was concluded that a five time increased annealing time resulted in a slightly increased oxidation thickness, and that the effect on elemental concentration was marginal, and that one hour was sufficient to reach steady state profile in $Ti_{1-x}Al_xN$ ($0 \leq x \leq 0.83$) coating. Available oxygen on surface diffused through vacancies and preferably reacted with Ti to form TiO_2, whereas released Al tended to diffuse towards the surface to form an Al concentration gradient. With increased x (higher Al content in the deposited film) the oxidation thickness decreased as the lattice supplied more Al and effectively reduced the thickness of TiO_2. The crucial role of Al content for a TiAlN film at different working temperatures, for example a cutting tool operation, was enlightened.

Oxidation behavior of four different PVD coatings was studied by Jx Chen [7] in 1997, where TiN and $Ti_{1-x}Al_xN$ (x-values of 0.008, 0.25 and 0.5) coated cemented carbides were tested. Furnace test (one hour in temperature ranges 200 – 800 °C),

Thermogravimetric analysis, machining and scratch tests were performed on these coatings. It was found that the TiN starts to oxidize at 500 °C and maximum rate at 750 °C and TiAlN with high Al-content starts at 800 °C and maximum rate at 950 °C. There was difficulty in finding oxygen on the machined tools, which is issued to investigate further.

M'Saoubi et al. [8] turned case hardened steel 16MnCr5 with TiN, TiSiN, TiAlN, AlCrN and uncoated polycrystalline cubic boron nitride tooling and compared their performance and wear modes. It was observed that the TiN degradation was caused by a combination of oxidation and plastic deformation of the TiN grans. TiSiN exhibit great wear resistance with its high hardness and thermal stability, though more brittle and is more prone to surface cracking. TiAlN is showing great wear resistance, the mechanical properties are improved during machining due to coherent isostructural spinodal decomposition and hardening, which is the essential contributor to the great wear resistance. The AlCrN is claimed as having great oxidation resistance and high hardness comparing to the other coatings, though displaying a lower crater- and flank wear resistance. TiAlN and AlCrN shows less workpiece adhesion compared to the others.

2.1.2. Workpiece material

The choice of material for a product or component has a big impact on the cutting performance, as well as on the machinability. The material decides which group of manufacturing processes is possible to use and the costs of the manufacturing method that comes with it. Ståhl [1] defines machinability of a material as follows:

"Machinability expresses how readily a particular workpiece material can be machined by a cutting tool in a manner such that certain predetermined levels of form, size, and degree of roughness of the surface can be achieved." [1]

A rough classification of metallic workpiece materials that can be used in metal cutting, are: [1]

- Cast ferrous alloys
- Steels
- Stainless steels
- Superalloys including those of titanium
- Non-ferrous alloys

The machinability of a workpiece material and physical characteristics affecting the cutting process can be assessed of 15 phenomena, which can be divided into even more subcategories. It is more common to include more of these phenomena in 5 different material factors to compare workpiece materials to each other: *abrasiveness, ductility, strain hardening, thermal conductivity* and *hardness.* [1]

Abrasiveness and proneness to wear, which is mentioned earlier in the tool wear section, is a material characteristic of, for example a multiphase material, which usually contains a phase with lower degree of machinability and another phase which is more brittle. The last one is commonly referred to as the β-phase of the material. For example, this can be controlled with the carbon content in a low-alloy steel, with lower carbon content than 0.3 % the material becomes more adhesive and with more than 0.5 % carbon the material becomes more brittle. [1]

Ductility, toughness or ultimate tensile strength, and adhesion are related to each other and makes the cutting process complex and difficult to predict. This phenomenon can be both an advantage and a disadvantage for the ability to machine the workpiece. If the material is ductile and has a high adhesiveness, this can be protecting the cutting edge if done in a stable way and extend its lifetime. If the adhered material is frequently removed though, this can lead to rapid and progressive wear of the cutting tool. [1]

Strain hardening, i.e. increase in yield strength during deformation, of the workpiece material means that there is a variation in the characteristics of it, which is usually due to that the machined surface of the workpiece gets hardened. This is usually occurring in deformation zone three and needs to be considered when machining more than one pass, as the load become higher on the cutting edge. [1]

Thermal conductivity of the workpiece material affects the process temperature with the *specific heat* having the proportionally strongest effect on the temperature. There is a difference of several tenths of degrees for the process temperature if the thermal conductivity is increased by 1%. As mentioned earlier, multiple factors, such as cutting forces, wear resistance and the power consumption are affected by the process temperature and the ability to transfer heat. [1]

Hardness and the deformation resistance of a workpiece material has a big connection to the cutting resistance of the material. With increased deformation resistance comes increased cutting forces and higher loads on the cutting tool. With multiphase materials, there is a variation in hardness that can be expected to have a variation in the cutting force as well. This might mean that there are short and segmented chips produced during machining which can be beneficial, with the hot chips easier being transported away from the contact zone and its surrounding, causing less interruptions in the manufacturing process and less damaged products. Chips are usually hot, and this energy will easier be transported away from the contact zone, where it is normally and advantage to keep the process temperature low. [1]

As explained above, workpiece materials vary a lot and comes with different challenges from a processing view. This report will not go deeper into detail of the different material factors, but rather focus on the workpiece used in this study and

the challenges with it: Alloy 718, or Inconel 718 – which is part of the *Superalloys including those of titanium* stated above.

Superalloys are generally of a big technical interest and is often used in components that require high corrosion- and oxidation resistance both at low and high temperatures. These materials are classified as being difficult to machine that result in high wear rates in cutting tools. Like in the case of Alloy 718, most superalloys are precipitation-hardened, which is performed by solution heat treated at a certain temperature, followed by rapid cooling and then aged at a set temperature. This leads to a high creep-strength in Alloy 718, which makes this material appropriate for use in applications in gas turbines, rocket engines, spacecraft, and nuclear reactors. Depending on the application, ceramic (recommended cutting speeds of 200 – 300 m/min and $h_1 < 0.15$ mm) or cemented carbide (recommended cutting speeds of 30 – 60 m/min and $0.20 < h_1 < 0.30$ mm) is commonly used as cutting tool material. [1]

Figure 2-10 compares the maximum tool interface temperature at different cutting speeds, which shows that titanium- and nickel alloys reaches high temperatures at relatively low cutting speeds. It should be noted that more advanced nickel alloys, like Alloy 718, are even harder to machine and generates more heat, than the ones shown in the figure. More advanced nickel alloys, strengthened by finely dispersed hard second phase as well as being age hardened, can be described as some of the most difficult materials to machine. These are designed to be highly creep-resistant, which is a challenging factor when machining this particular material. [9]

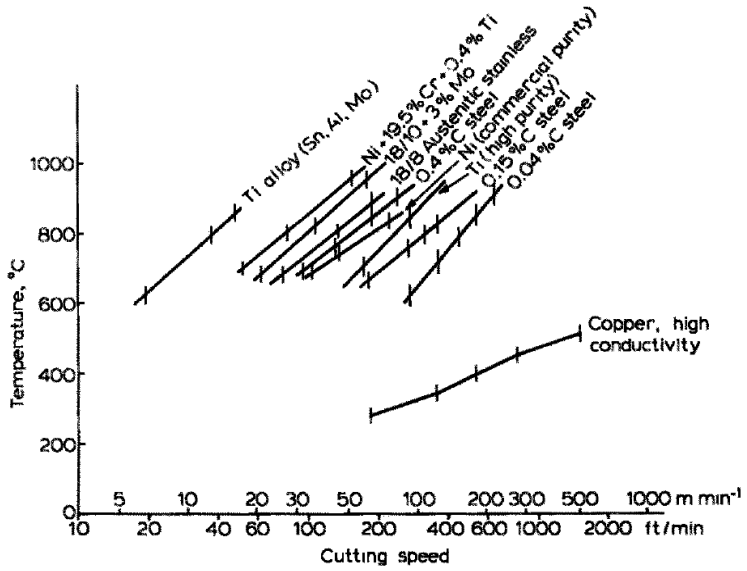

Figure 2-10 Maximum interface temperature, for high speed steel tools, depending on the cutting speed. [9]

Adhesion of workpiece material is a challenge when machining Alloy 718, and it has consequences which are mainly seen as problematic and damaging to the machining process. Something that has been found to be hard to investigate but that is of big interest, is if the adhesion effect could be done in a controlled way and without damaging the tool. Finding a way when adhered workpiece material protects the tool, and is supplied continuously during the cutting process, would be ideal and have a strong effect on the tool life. [1]

2.1.3. Tool material

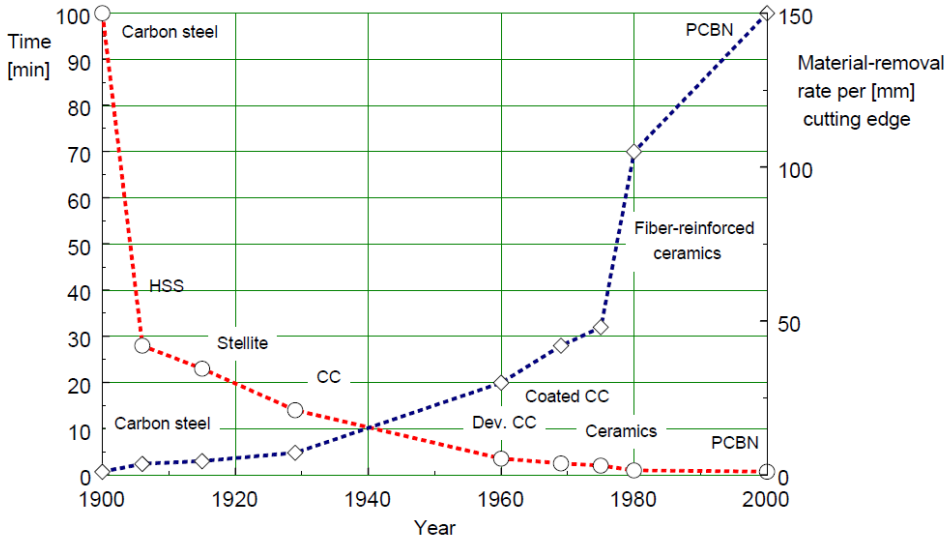

Figure 2-11 Historical development of different materials that cutting tools can be composed of, with the red line showing the relative time required for a particular processing step and the blue line showing the relative processing capacity of the tool in terms of cm^3 chips per minute for each mm of the cutting edge. The carbon steel provides reference values for comparison. [2]

In the beginning of the last century, many discoveries and innovations were made in the development of tool materials, which can be seen in Figure 2-11 above, that played a big role in industrial development. A major advance was when high speed steel (HSS) replaced carbon steel as cutting tool material, which, for example, played a central role for the mass production of vehicles. HSS is still an important tool material today. Cemented carbides (CC) were originally commercialized in 1929 by the German industrial concern Krupp. In Sweden, commercial production was introduced by Fagersta Bruk (Seco Tools AB today) in 1932 and by Sandvikens Jernverk (Sandvik Coromant today) in 1942. Another big innovation step was done by Sandvik Coromant in 1969 when they coated cemented carbides with, initially, titanium carbide. Later, other substances of coating materials were used, which have played a major role in modern cutting tool development. [1]

The main requirement of a cutting tool material is that it must be harder than the material which will be machined by it. It is well known that the tungsten carbide is

one of the hardest carbides, and it was found that iron powder worked well as binder material when sintering tungsten carbide. Iron was soon replaced by cobalt, which is still the basic composition used today. By developing better manufacturing techniques, the performance of the cemented carbide could be improved. The tensile strength, for example, has been increase from about 1000 N/mm^2 in the 1930s to about 3000 N/mm^2 today. [1]

Cemented carbides represent a group of composite materials that are characterized by the high wear resistance and high level of hardness and strength. These are powder-metallurgically manufactured and usually consist of hard particles that are sintered together by a metallic binder. All cemented carbides contain tungsten carbide (WC), as the most important hard phase, often together with another carbide, carbonitride or nitride of titanium, niobium, vanadium or chromium. Nickel and iron can be present as the binding metal, but cobalt is the most usual one. By changing the content of the hard phase and the binding metal can be done to suite the desired application, for example by increasing the binder content, the toughness is increased. By increasing the amount of hard particles, the hardness and abrasive wear resistance can be increased. Table 2-1 shows examples of different compositions and their practical applications. [1]

Table 2-1 Example of bulk composition in volume percent and grain size ρ_{tm} for different types of cemented carbide according to ISO 513 intended for different areas of application. [1]

	ISO 513	% WC	% TiC	% TaC+ % NbC	% Co	ρ_{tm} [µm]	Practical application
1	P10	70	14	8	8	2-3	Finishing of long-chipping steel
2	P30	75	7	8	10	2-3	Medium-roughing of long-chipping steel
3	P40	75	5	8	12	1-3	Roughing of long-chipping steel
4	M10	87	2	3	8	1-2	Finishing of stainless steels
5	M40	85	2	3	10	1-3	Roughing of stainless steels
6	K10	91	2	1	6	1-2	Finishing of short-chipping materials
7	K40	88	0.5	0.5	11	2-3	Roughing of short-chipping materials

2.1.4. Coatings

As mentioned above, a big innovation step for cutting tools were made in 1969 when Sandvik Coromant coated cemented carbides with titanium carbide. Coatings are used to increase the wear resistance of the cutting tool, where ceramics of oxides, nitrides and carbides are the most common coating material. The typical characteristics of ceramics are the stability at high temperatures, chemically inertness, high hardness, and brittleness. These characteristics supports the, in general, softer substrate material. [1]

One reason for a big portion of indexable cutting tools being coated today is the ability of extending the tool life by a factor of 2 or 3, by reducing the wear rate when

high speed turning cast iron and steel. Some users increase the speed by 25 % up to 50 %, without reducing the tool life. [9]

There are mainly two deposition techniques used when coating cutting tools, which are Chemical vapor deposition (CVD) and Physical Vapor Deposition (PVD), described below in separate chapters. There will be more focus on the PVD technique due to the subject of this master thesis.

2.1.4.1. CVD – Chemical Vapor Deposition

The chemical vapor deposition is a technique where one or several metals, in a chloride form, for example $TiCl_4$ and $AlCl_3$ which are in gaseous state at relatively low temperatures, are brought in contact with the surface of the cutting tool in a chamber. The chlorides are absorbed by the surface of the coating and together with hydrogen, being present in the chamber as well, hydrochloric acid and chlorine are formed and pumped out of the chamber. Nitrogen, carbon and the acid react with the metal and form a ceramic layer. This takes place at 800 – 1000 °C in a stress-free environment, and when cooled to room temperature, tensile stresses are developed in the coating due to difference in the heat expansion coefficient between the substrate and the coating. The CVD techniques provide a coating thickness of 4 – 20 μm and provides a high level of resistance toward abrasive wear. [1]

2.1.4.2. PVD – Physical Vapor Deposition

The physical vapor deposition is a so-called focused process, where the metals are taken from a "target" by vaporization which is then transported to the cutting edge. Only the parts of the tool that are directly exposed to the metal flux will be coated, and the metal atoms then react with the gases in the chamber to form a ceramic coating. One PVD method, used in this master thesis, is cathodic arc evaporation, in which the metal flux is highly ionized. With the metal ions being accelerated by a negative potential applied to the cutting tool, it gets bombarded by the high-energy ions and compressive stress is developed on the surface. This takes place in reduced gas pressure and at temperatures of 400 – 600 °C. With the PVD process the typical thickness range is 1 – 5 μm, which is beneficial for tools used in finishing operations, which maintain the sharp edges needed for that kind of application. [1] [9]

2.2. Microscopy methods

In this section, methods that was intended to be used in this master thesis are described briefly.

2.2.1. Scanning Electron Microscopy (SEM)

With optical microscopes having an upper magnification limit of about 2000 times, structural elements are too fine to observe and at higher magnification electron microscopes are used. These use electrons instead of light and focused electron

beams with short wavelength and images can be formed by magnetic lenses. SEM is an investigative tool that can examine a specimen with an electron beam, secondary or back-scattered electrons are collected to create an image representing the surface features. The investigated specimen must be electrically conductive, otherwise a thin metallic surface coating must be applied. With SEM equipment, it is possible to reach a magnification range of over 50'000 times. [4]

A big development in recent years has been the gathering of chemical composition of a specimen, by bombarding it with high-energy electrons, which then emits X-ray characteristics of the specimen. This radiation can be measured with a detector which can produce a voltage pulse that is proportional to the energy of the incident's photons. This method is called energy-dispersive x-ray spectroscopy (EDX) and can be used to make an analysis of the elemental composition of a highly localized area. [10] [11]

2.2.2. X-ray Diffraction (XRD)

X-ray diffraction, referred to as XRD, have historically been used to understand the atomic and molecular arrangements in solids. This technique is still important for the development of new materials to decide the crystalline structure. A beam of focused X-rays onto a sample diffracts a pattern, which is measured by a detector at a specific angle, called the diffraction angle. This diffracted pattern gives characteristics of the wanted sample, with the possibility to decide unit cell size and geometry, arrangement of atoms in the unit cell, qualitative- and quantitative chemical identifications and determination of residual stresses. [4]

2.2.3. Thermogravimetric analysis, TGA

This is a method to characterize materials used in different environments, by measuring the mass of the substance, which is monitored as a function of either temperature or time. A sample is subjected to a controlled temperature program in a controlled atmosphere, which can be of both an inert or a reactive gas that flows over the sample and out through an exhaust, while the weight is observed. Thermal analysis of a material is considered to be a complement to XRD, optical- and electron microscopy when developing a new material and can be used to define temperature and energy changes connected to structural changes in the material. [10]

3. Method

This part of the report describes all steps, based on the theory and the different analysing methods that were planned to be used. A method plan was initially formed but due to circumstances and time management, and as the results progressed, the plan got redesigned and some steps were added, and some were excluded.

3.1. Original overview plan

The planned methodology for the project and steps needed to answer the problem description.

3.1.1. Thermogravimetric analysis - TGA

The coating material should be manufactured in such way that it is possible to make thermogravimetric analysis on it. This is not possible with the cemented carbide as substrate, when temperatures way beyond the working area of it, should be tested. There are options which should be investigated and decided.

When the manufactured part is complete, a test program needs to be set for all coatings, which needs to be motivated by findings from similar experiments and what temperature range is reasonable to try for the materials used in the coatings tested in this project.

In this work a temperature profile of the coating materials should be established and compared. This is to find, for example, at which temperature the different coatings start to oxidize, certain temperature when it rapidly oxidizes and other behaviours.

3.1.2. Furnace tests

Furnace tests can be used to subject a sample to different temperatures and/or atmospheres in order to study reactions after cooling down of the sample. This would probably give a first indication of the appearance of protective oxide scale, rapid growth of weak oxides or resistance against oxidation. Compared to the TGA, the substrate material might also react with the coatings at elevated temperatures.

In this work a certain temperature, or temperatures, should be tested and compare the ability of protecting the substrate from oxygen, at temperatures that can be reached during machining.

3.1.3. Machining

To connect the results, from experiments in furnace and TGA, to see the relevance of it and how it works during metal cutting, machining experiments should be performed. Two different kind of machining strategies should be performed:

3.1.3.1. Short time, elevated speed

This test should be designed to make sure that reactions will occur on the surface of the coating, whilst keeping it intact, by machining at elevated speed and short time in contact with the workpiece. If successful, it should be possible to have a look at the surface of the tool, where the coating is supposed to be in good shape, and see what products are formed in the process. With the previous steps above, this can help understand the result and to confirm, or show that something else happens, in practical use and in contact with a workpiece.

3.1.3.2. Performance test

This test should be designed to be as close to a realistic case with cutting parameters like the ones used in industry, to show whether the results shown in previous steps makes the tools stronger and giving a longer tool life or not. A certain wear criterion will be decided, and the tool should be used in short steps and measured to see how long time it takes before reaching this criterion.

3.1.3.3. Environments

To understand behaviours and reactions on the surface of the coating, different environments will be used during turning, with methodology like the research mentioned in 2.1.1. [5]

3.1.4. SEM

Samples should be analysed with SEM equipment to scan tools, used as well as new tools. Visually changes can be found, and EDX technique provides information on elemental composition on as-worn tooling.

3.1.5. XRD

XRD can be used as a technique to identify phase compositions of the elements confirmed in EDX analysis. This will be done on the coatings which performs the best and might not be done for the whole setup.

3.2. Outcome

As the results progressed, the planned methodology was reworked, and some techniques were excluded while some were added. The actual method outcome is presented below.

All tools, with different geometries, used in this project were of substrate material cemented carbide, WC-6 wt% Co.

3.2.1. Coatings

Four concept coatings were manufactured, with the content being designed to match the workpiece material. The material content and manufacturing method are confidential, and will therefore be referred to as coating C1, C2, C3 and C4 onwards. Two reference coatings, TiN and TiAlN, were used as comparison of the performance of the concept coatings.

Figure 3-1 shows the setup of foil and tools mounted in the PVD furnace used to deposit the coating. Three reference tools, to the right of the foil, were used to verify that desired quality of the coating is reached.

Figure 3-1 Foil and tools mounted at a specific level in the PVD furnace.

3.2.2. Thermogravimetric analysis - TGA

For TGA analysis, two method options could be identified:

1. Coat a sample, which needs to be of a substrate material that is stable up to about 1100 – 1200 °C and is possible to deposit with PVD technique, that fits in the chamber of the Netsch with volume and weight limits stated in chapter 2.2.3.
2. Coat a thin magnetic foil, dissolve the foil and filter out the coating in a few steps.

With a small window of substrate material working for the first option and with availability to perform the latter option, the second option was chosen. Foil was mounted in the furnace together with the tools, as can be seen in Figure 3-1. The iron foil went through a dissolving process where the iron gets boiled away in a solute, which then was filtered and only left the coating in a powder form. The dissolving process was made by chemical experts at Seco Tools AB.

Due to delay, in the manufacturing process of the coatings, the powder was not further analysed, with the powder arriving after the first machining tests were done and instead other experiments were prioritized.

3.2.3. Furnace test

The coated tools were heated in an oven to study the influence of oxygen on the coatings at elevated temperature. Tools used for furnace tests were of ISO insert geometry TPUN160308 which has a flat top surface that facilitate some of the microscopy methods. For the C4 experiment a set of ISO geometry CNMA120408 tools were used, which would not be used for machining due to manufacturing issues.

3.2.3.1. C4 experiment

Two studies, by Greczynski et al. [6] and by Jx Chen [7], gave a hint of interesting temperature spans to test on the coating materials. It was decided to experiment with the first available coating, which was the C4, and see what happened at 600 °C, 700 °C, 800 °C and 900 °C respectively, one tool for each temperature during 30 minutes.

The tools were placed to cool down in air until they reached room temperature. With visual inspection and the results from literature study it was decided to cut the 800 °C tool to study the cross section in SEM.

3.2.3.2. 800 °C for 1 hour

With the results from the C4 experiment, it was decided to put one tool of each coating, Figure 3-2, in the furnace at 800 °C for 1 hour. This because the C4 appeared oxidized on the whole surface which it did not for the lower temperatures, and that 900 °C probably would be beyond the limits of the TiN coating. 800 °C was concluded to be the sweet spot when the coatings should survive and the TiAlN coating also would react at this temperature, which probably has the highest oxidation resistance.

Each tool was marked with a number (1 – 6) on the top surface, to make sure they would be recognizable in case of an accident or a major change of the tool. The crucible was placed in room temperature to cool down. All six tools were cut and prepared, with the tool preparation steps described below, before bringing them to the SEM.

Figure 3-2 Coating C1, C2, C3, C4, TiN, and TiAlN before being exposed to 800 °C for 1 hour.

3.2.4. Machining

SMT SAJO, 500 Swedturn, CC 4100, NC-turning lathe was used for machining tests in this report. Solution and precipitation treated Alloy 718 was used as workpiece material for all machining tests in this study. The composition measured by the manufacturer is presented in Table 3-1 Chemical composition of Alloy 718, tested by supplier Special Metals.Coated ISO insert geometry CNMA120408 tools were used in machining experiments in this study.

Table 3-1 Chemical composition of Alloy 718, tested by supplier Special Metals.

Element	Maximum %	Test Result %
Ni	55.0	53.0
Cr	21.00	19.34
Fe	-	17.5
Nb	5.50	5.17
Mo	3.30	2.99
Ti	1.15	0.95
Al	0.80	0.48
Co	1.00	0.32
Mn	0.35	0.08
Cu	0.30	0.06
Si	0.35	0.06
C	0.08	0.03
Ta	0.05	<0.01
P	0.015	0.009
B	0.006	0.004
Se	3 ppm	< 3ppm
Pb	5.000 ppm	<0.200 ppm
Bi	0.3 ppm	<0.1 ppm

Two different approaches, with different cutting conditions, were performed. The first with the objective of machining at high speed for a short time, to speed up the reactions in the tool- workpiece interface. The second approach was designed to have industry-like cutting conditions to compare the wear rate of the tools. The two approaches included machining both in high pressure air and in high pressure argon, which were adjusted to have approximately the same pressures for both environments.

3.2.4.1. Elevated speed

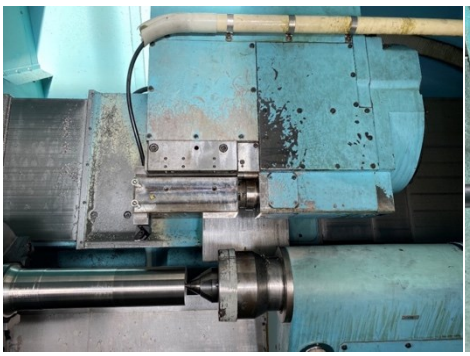

Figure 3-3 Machining setup, elevated speed.

Figure 3-4 Tool holder setup, elevated speed.

Seco Jetstream tool holder DCLNL2525X12JETI was used for the elevated speed test, with setup shown in Figure 3-3 and Figure 3-4. This 3D-printed head has nozzles close to the edge of the tool on the rake side and a nozzle on the flank side. This setup maintained a pressure of approximately 4 bars during machining, both for air and argon.

As described above, this test was designed to reach high temperatures which meant that elevated cutting speed was needed. To find conditions suited for this setup and tools, TiAlN coating was used to find conditions with the objective speed around 200 m/min and time in contact of about 5 to 10 seconds. Different speeds were tested, and the tools were visually inspected in an optical stereo microscope, Olympus Stream Basic SCZ7. These were scanned in an Alicona Infinite Focus microscope as well to confirm that the coating was still intact. It was important to have a big contact area to be able to analyse the reactions on the surface, this concluded with the cutting conditions stated in Table 3-2.

Table 3-2 Cutting conditions, elevated speed.

Cutting speed, v_c	**Feed, f**	**Depth of cut, a_p**	**Time in contact, t**
200 m/min	0.15 mm/rev	0.5 mm	5 sec

All coatings were first tested in air, and every test was run twice to have two sets of tools to analyse, with the possibility of sending one set to another location for special analysis. The argon equipment were then installed, and same tests were done another two times for each coating.

3.2.4.2. Performance test

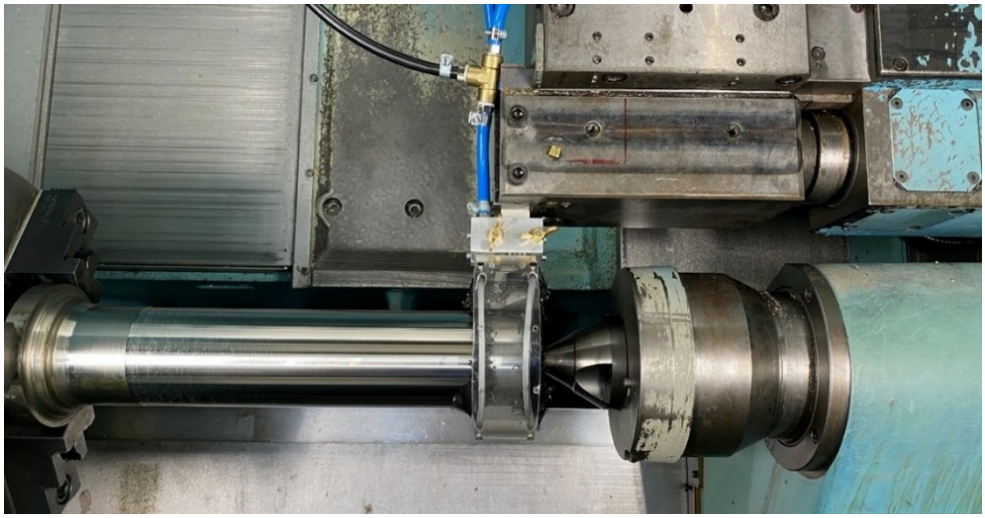

Figure 3-5 Machining setup, performance test.

With the results from the high-speed tests, and the uncertainty whether an oxygen free environment in the contact zone is reached only with the argon flow from the tool holder nozzles, a controlled environment chamber was installed. This chamber has extra nozzles in the chamber, which has been used for similar experiments at the Production and Materials engineering division, see [5]. Due to these extra nozzles the pressure into the system was around 2 bars.

To find appropriate cutting conditions, the TiAlN coating was tested in similar way as described above in the elevated speed experiment, with the objective of reaching flank wear VB_{max} = 200 µm after 5 – 7 min. The same depth of cut and feed rate was used. Tests performed in this chamber were done in 30 seconds interval and measured with optical microscope, to find when the wear criterion was reached. Different speeds were tested and concluded with cutting conditions stated in Table 3-3.

Table 3-3 Cutting conditions, performance test.

Cutting speed, v_c	**Feed, f**	**Depth of cut, a_p**	**Maximum flank wear, VB_{max}**
60 m/min	0.15 mm/rev	0.5 mm	200 µm

All coatings were tested in air until the maximum flank wear measured 200 µm, to compare the results in argon the same machining time was performed in argon in 30 second steps.

3.2.4.3. C4 short time test

The same cutting conditions as the performance test, Table 3-3, were used and three different runs were performed: 10, 20 and 30 seconds respectively, in high pressure air. These tools were prepared, as described in the Tool preparation steps below, and brought to the SEM for imaging and measurements of the wear.

3.2.5. Tool preparation

Thermally exposed tools, from furnace tests, were cut, a small part of the tool was mounted in epoxy and polished to be able to look at the cross section of the tool. The cutting procedure was done in a Struers Accutom-100 with a diamond disc at 3000 rpm and 0.05 – 0.2 mm/rev feed. The tools were forged in a Struers CitoPress-5 in polyfast material. The samples were then polished in different steps depending on the state of surface that were to be investigated.

For machined tools, the position of the cross section was critical, and a couple of trials were performed to make sure that the surface of the coating would not be affected by the preparation steps and to get to a wanted position. By cutting the tools, with conditions described above, at a position similar to what is done in Figure 3-6, with the cutting tool mounted in a holder which was brought from the saw to the optical microscope to measure the distance from the cut to the middle of the contact zone. The cutting diamond disc was replaced with a diamond grinding wheel and ground to the wanted position, with the finished result shown in Figure 3-7.

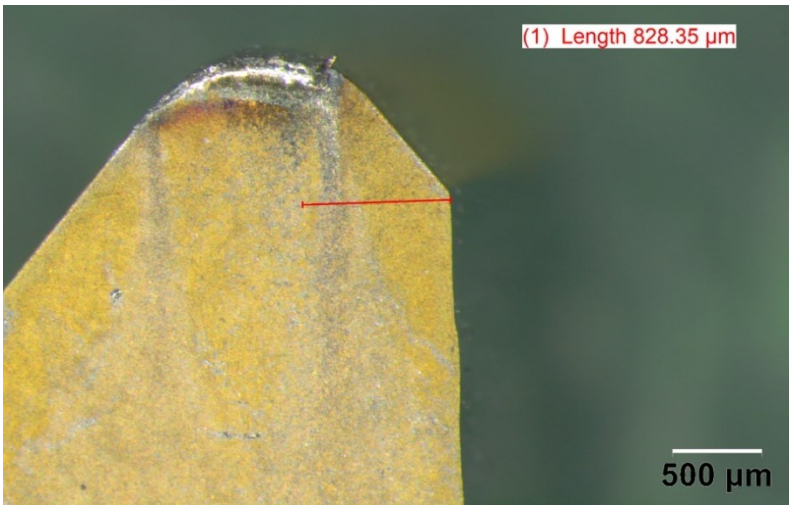

Figure 3-6 Example of result after cutting tool and measure in optical microscope.

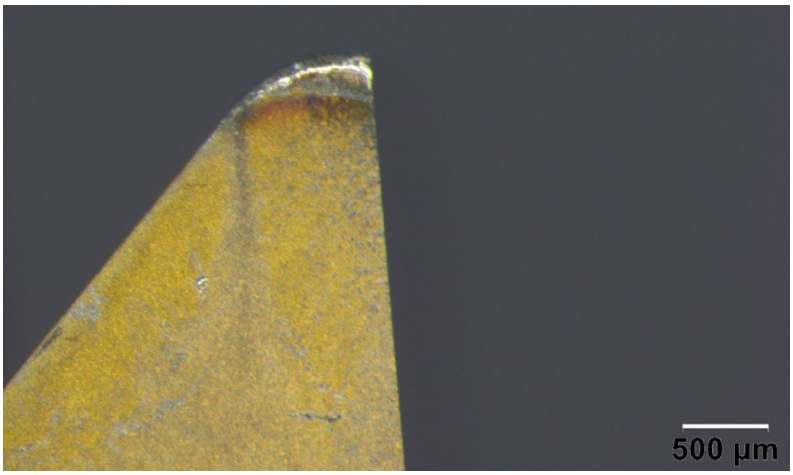

Figure 3-7 Example of ground tool to a certain position.

3.2.6. SEM

SEM analysis were performed with a Tescan Mira3 High Resolution Schottky FEG-SEM equipped with an Oxford EDX system at the Department of Geology, Lund University. Samples were cleaned with isopropanol and dried with nitrogen gas before installation in the chamber.

4. Results

In the following chapter the results are presented which includes the result from the TGA procedure, furnace- and machining experiments.

4.1. Thermogravimetric analysis - TGA

The coating was successfully deposited and dissolved. The amount of powder was less than expected which could have been challenging to work with. Due to time priority this analysis was not proceeded further.

4.2. Furnace test

Results of the tests done in furnace.

4.2.1. C4 experiment

Four different temperatures were tested on C4 concept coating with the visual result shown in Figure 4-1, each for 30 minutes. The tool being in the furnace at 800 °C was decided to have a deeper look at. This since the 600 °C and 700 °C tools are oxidised on the edges, judging from the colour changes, and the 800 °C tool appears oxidized over the whole top surface. With this experiment being done to find the optimum temperature to test for the rest of the coatings, the objective is to find a sweet spot where the coatings oxidise on the whole top surface, but not all the way through the coating's depth.

The 800 °C tool got prepared with the described steps above, and brought to SEM, result shown in Figure 4-2.

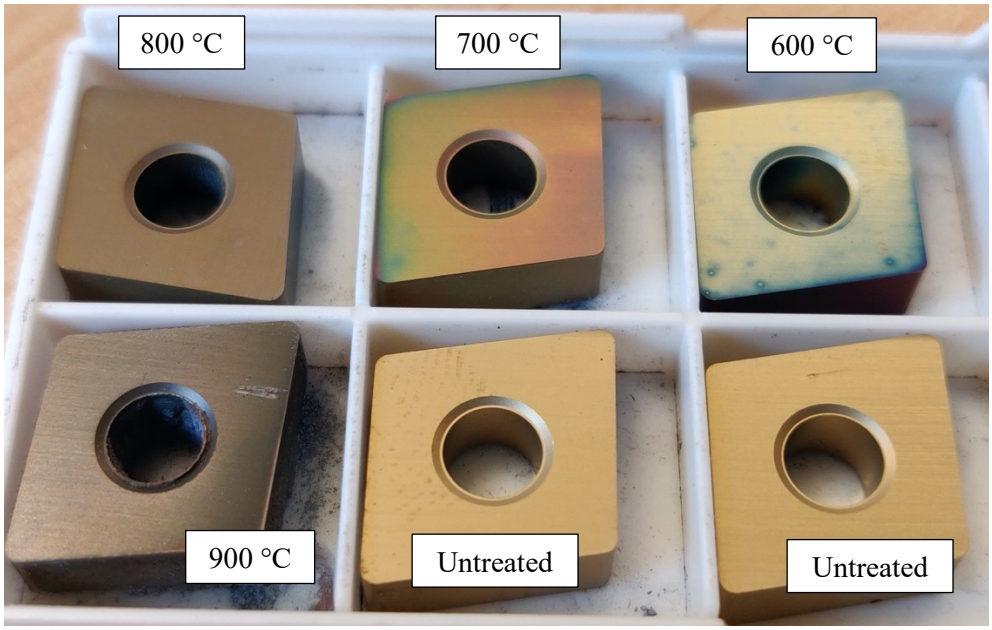

Figure 4-1 Test of different temperatures for 30 minutes. Two tools in original shape.

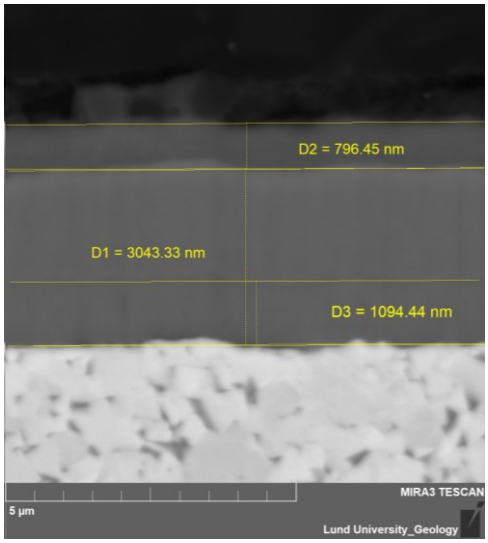

Figure 4-2 Back-scattered electron image from cross section of C4 tool after 30 min in furnace at 800 °C.

An oxidation layer of 0.8 µm was measured, which is about 21% of the total coating thickness. This should not be compared with the thickness of the results below since this tool was from an early manufacturing batch with larger thickness compared to the coatings used below.

4.2.2. 800 °C for 1 hour

The tools were thermally exposed in air at 800 °C for 1 hour and cooled down in room temperature in the crucible. The visual result is shown in Figure 4-3, which can be compared with before shown in Figure 3-2.

C1 coating probably oxidized all the way to the substrate, which resulted in the coating to create a crack all around the edge line. When preparing the tools, the oxidized coating loosens from the tool and could not be fully prepared for SEM microscopy. With machining experiments performed in parallel with this, C1 and C2 performed significantly worse compared to the other coatings, and were not tested further after this stage.

Figure 4-3 Furnace samples placed from the left: C1, C2, C3, C4, TiN and TiAlN, after 1 hour in 800 °C.

With the concept coatings content being classified, EDX scans of these coatings will not be presented in this report. For the TiN and TiAlN coatings, both back-scattered images and EDX scans will be presented in the following sections.

4.2.2.1. TiN

SEM and EDX results, Figure 4-4 and Figure 4-5, show that the TiN coating has oxidized almost all the way to the substrate material. An oxidized thickness of about 5.0 µm is measured, which means that the coating has more than doubled in thickness, from the original coating thickness of about 2.3 µm.

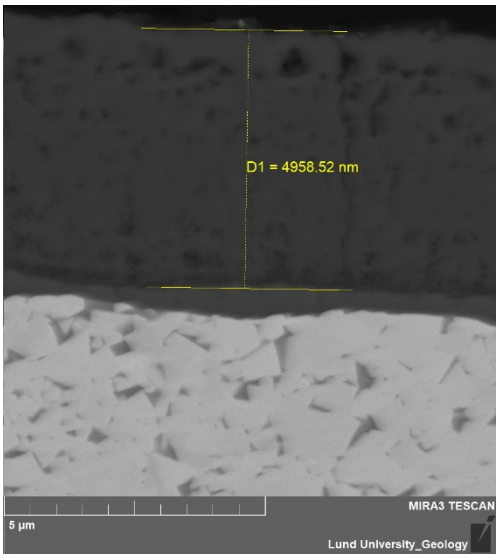

Figure 4-4 Back-scattered electron image of TiN, cross section, after 1 hour in furnace at 800 °C.

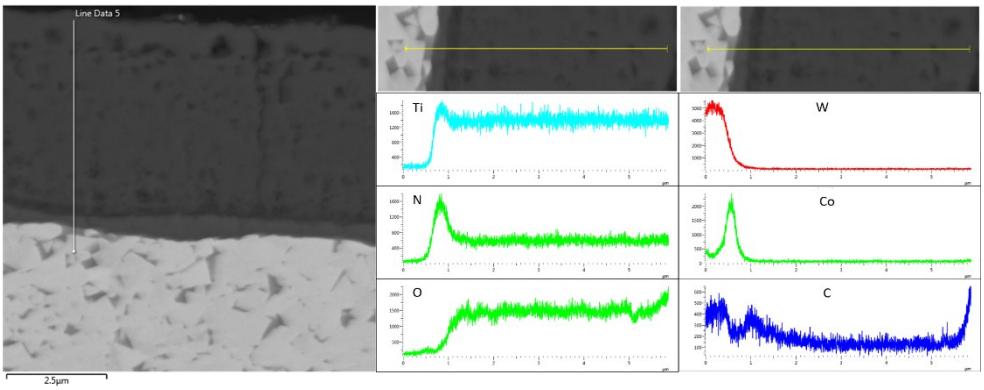

Figure 4-5 EDX of TiN, cross section, after 1 hour in furnace at 800 °C.

A spot was found, Figure 4-6, where oxygen has reached the substrate material and parts of the tungsten and cobalt appears to have diffused into the coating and started to travel to the surface.

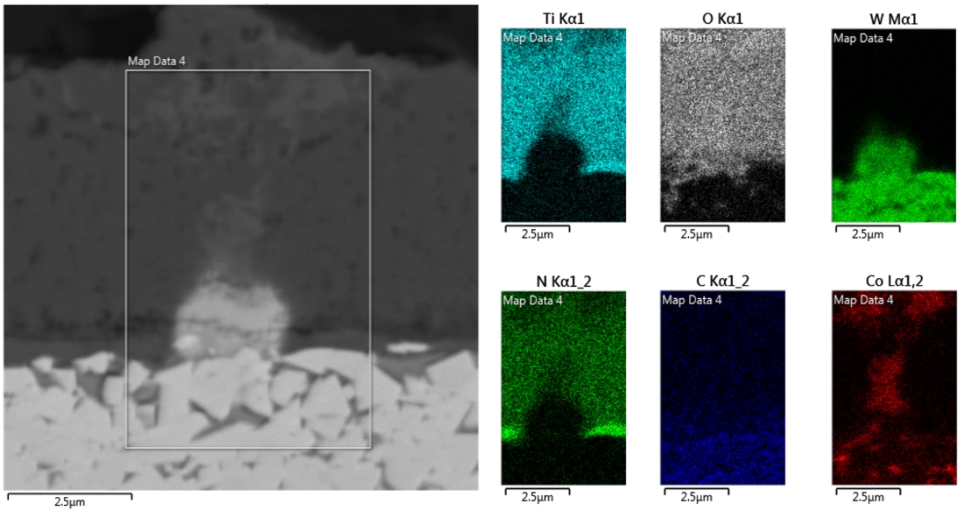

Figure 4-6 EDX of TiN where oxygen has reached the substrate material.

4.2.2.2. TiAlN

SEM and EDX results, Figure 4-7 and Figure 4-8, shows that there is barely any oxidation found in the TiAlN coating. The oxygen signal was weak and considered as insufficient. The thickness of the coating is not affected with this test.

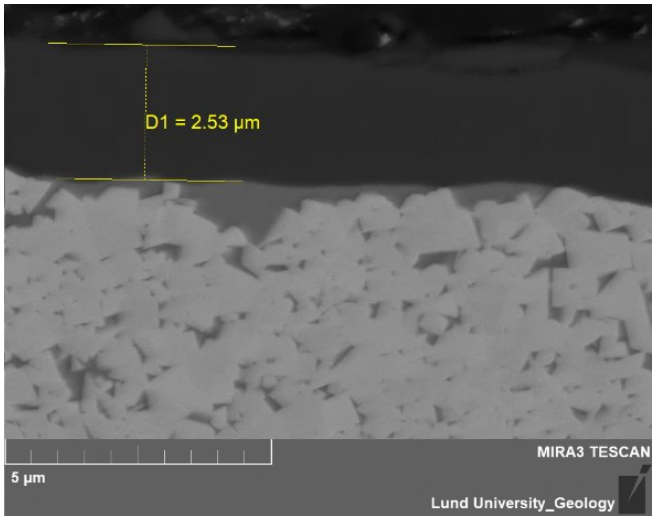

Figure 4-7 Back-scattered electron image of TiAlN, cross section, after 1 hour in furnace at 800 °C.

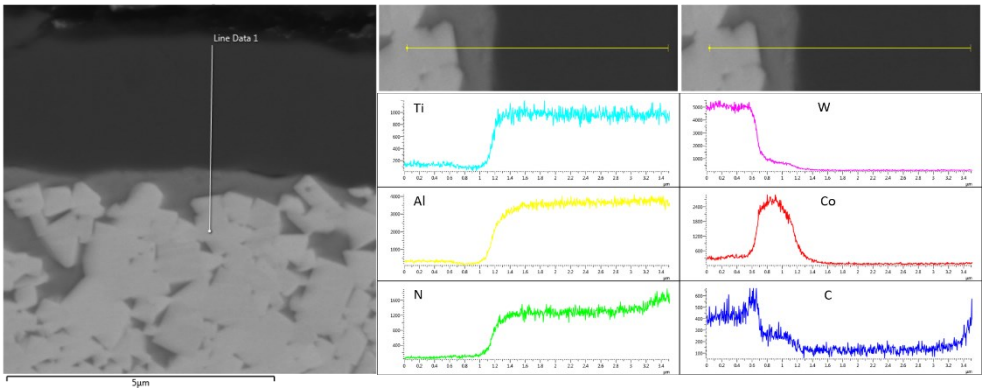

Figure 4-8 EDX of TiAlN, cross section, after 1 hour in furnace at 800 °C.

4.2.2.3. C3

SEM scan, Figure 4-9, show an oxidation film forming on the top of the coating, measured to a thickness of 0.3 µm. The thickness of the coating has grown slightly, from 2.5 to 2.7 µm.

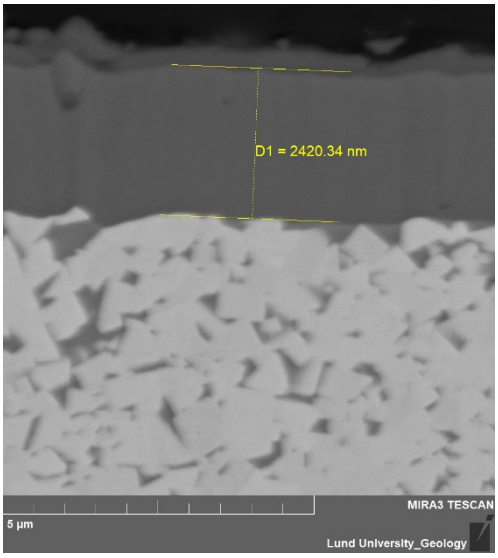

Figure 4-9 Back-scattered electron image of C3, cross section, after 1 hour in furnace at 800 °C.

4.2.2.4. C4

SEM scan, Figure 4-10, show an oxide scale, 1.6 µm, about as thick as the non-oxidized part of the coating, 1.8 µm. The coating thickness has increased from 2.6 µm to 3.4 µm.

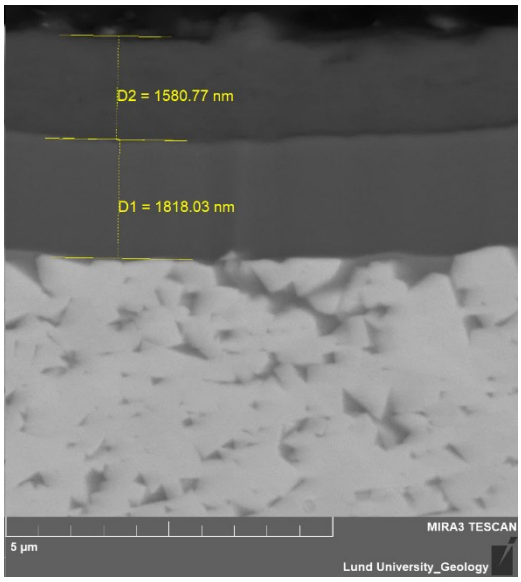

Figure 4-10 Back-scattered electron image of C4, cross section, after 1 hour in furnace at 800 °C.

4.3. Machining

Results from the machining tests, including Elevated cutting speed, Machining Performance test and extended C4 testing, are presented below.

With the material content of the concept coatings being classified, EDX scans of these coatings will not be presented in this report.

4.3.1. Elevated speed

Results from machining with elevated cutting conditions, as stated in 3.2.4.1. Figure 4-11 illustrating an example of the tools surface and shows the rake face of the cutting edge. The contact zone between the workpiece and the tool marked with red, adhered material on the edge line marked with yellow, some adhered material and debris is generally found in the area marked with green (referred to as being *outside the contact zone*). There are a few cases where an area of the substrate material can be seen and the coating is worn and gone, marked with blue.

It should be noted again that these tools, showing the surface, were etched before being scanned in the SEM. As the results will show below, there are still adhered material found on the surface, with the etching process removing some adhered material but not completely. With this in mind, the EDX results will be look at but cautiously compared.

Cross sectioned tools have not been etched.

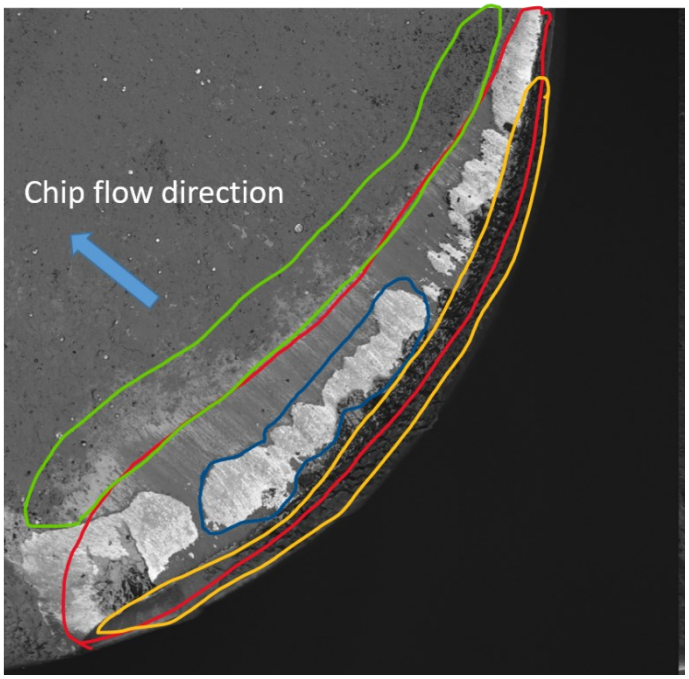

Figure 4-11 Example of scanned rake face surface with areas of interest.

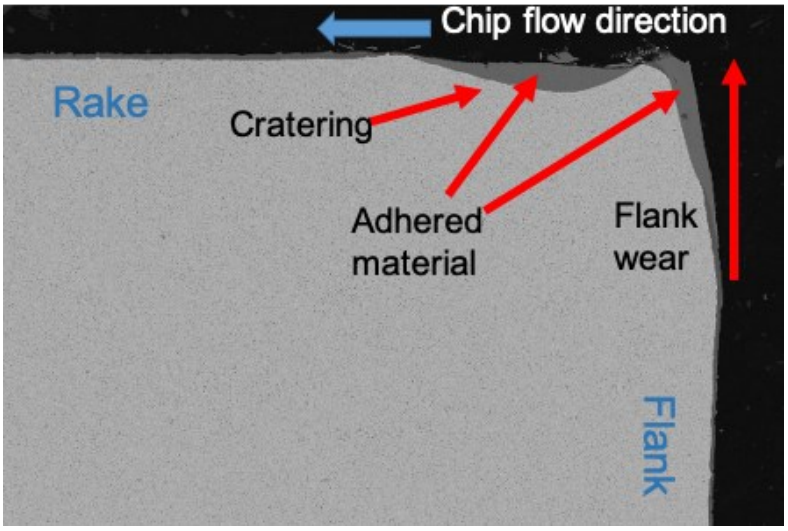

Figure 4-12 Example of cross sectioned tool with wear behaviours of interest.

Figure 4-12 shows the principal for scanned results of the cross sectioned tools, where wear behaviours like cratering, flank wear and parts of adhered material are marked. All cross sectioned results, if nothing else is mentioned, will be presented in this way.

4.3.1.1. TiN

Figure 4-13 shows the rake face of the TiN cutting edge machined in HP air, in the contact area with the workpiece, the coating is mostly gone. On the very edge there is adhered workpiece material. Outside the contact zone it appears to be more debris compared to the edge machined in argon, Figure 4-14. More of the contact zone appears intact when machined in argon.

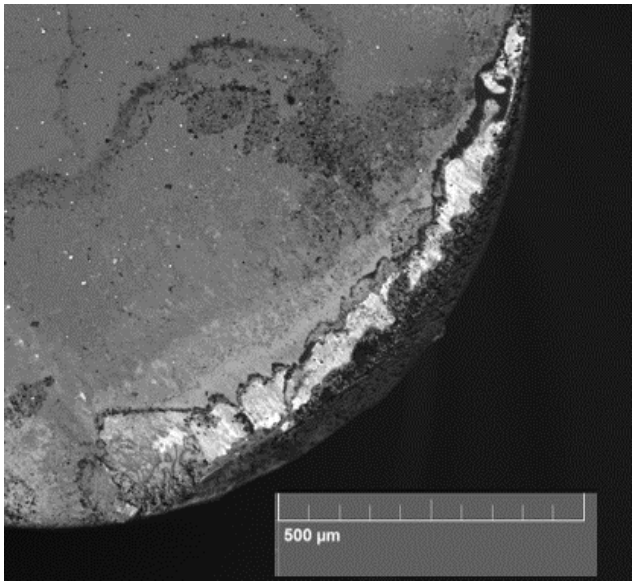

Figure 4-13 Back-scattered image of TiN surface, machined 5 seconds in HP air at v_c = 200 m/min.

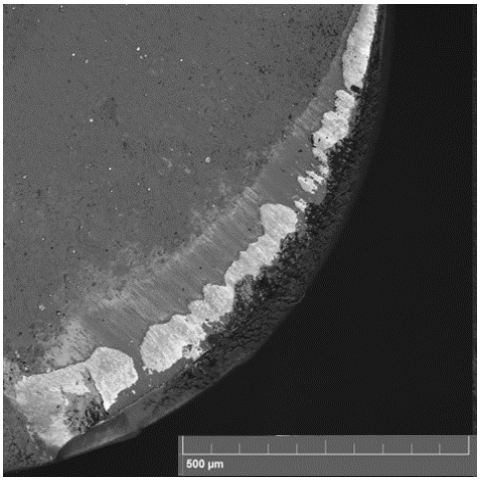

Figure 4-14 Back-scattered image of TiN surface, machined 5 seconds in argon at v_c = 200 m/min.

Scanning the surface of the TiN coating, Figure 4-15 and Figure 4-16, shows that there is still some adhered material (Ni, Nb and Cr), both on the coating and on the substrate where the coating is worn away, seen in the brighter parts of the images.

Cr and O have EDX peaks close to each other and might interfere each other, especially when there is a low amount of the substance, as in this case.

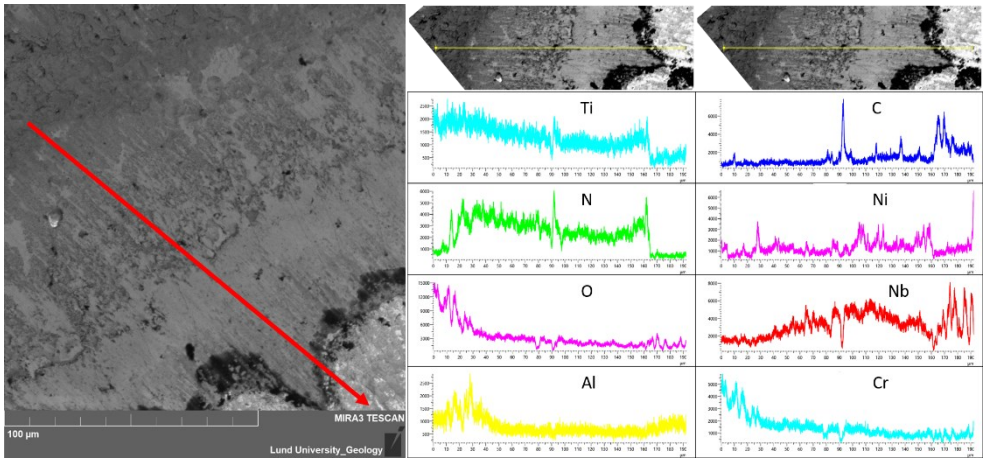

Figure 4-15 Surface EDX of TiN, machined 5 seconds in HP air at v_c = 200 m/min.

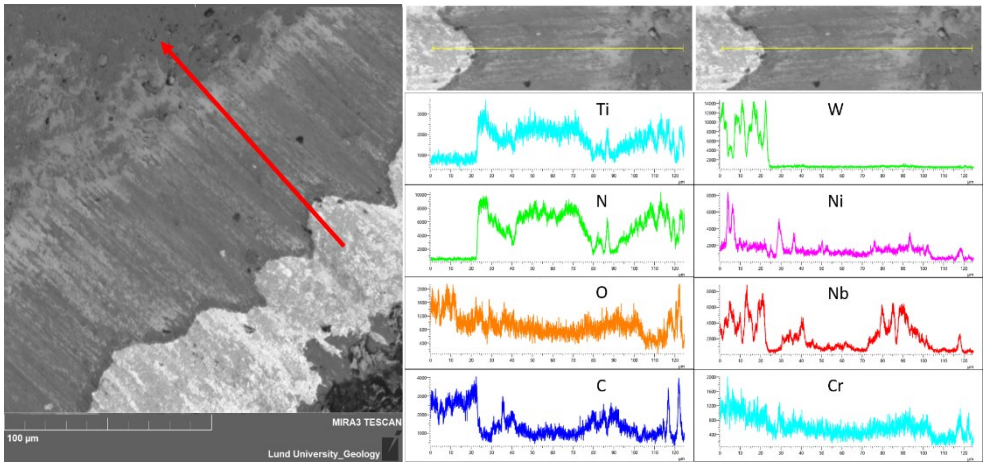

Figure 4-16 Surface EDX of TiN, machined 5 seconds in argon at v_c = 200 m/min.

Cross section images, Figure 4-17 and Figure 4-18, show some flank wear on both tools, and the coating is absent in these regions. The substrate is the brightest material seen in the images, with the coating appearing the darkest and adhered material in between these two. There is an initial cratering seen in both cases, where the coating is worn away.

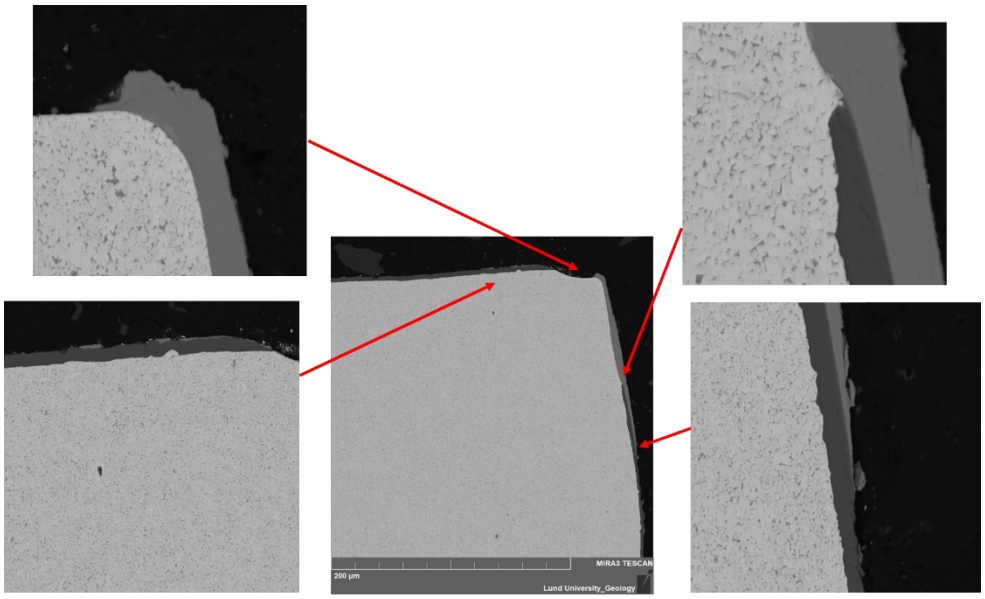

Figure 4-17 Cross section of TiN, machined 5 seconds in HP air at v_c = 200 m/min.

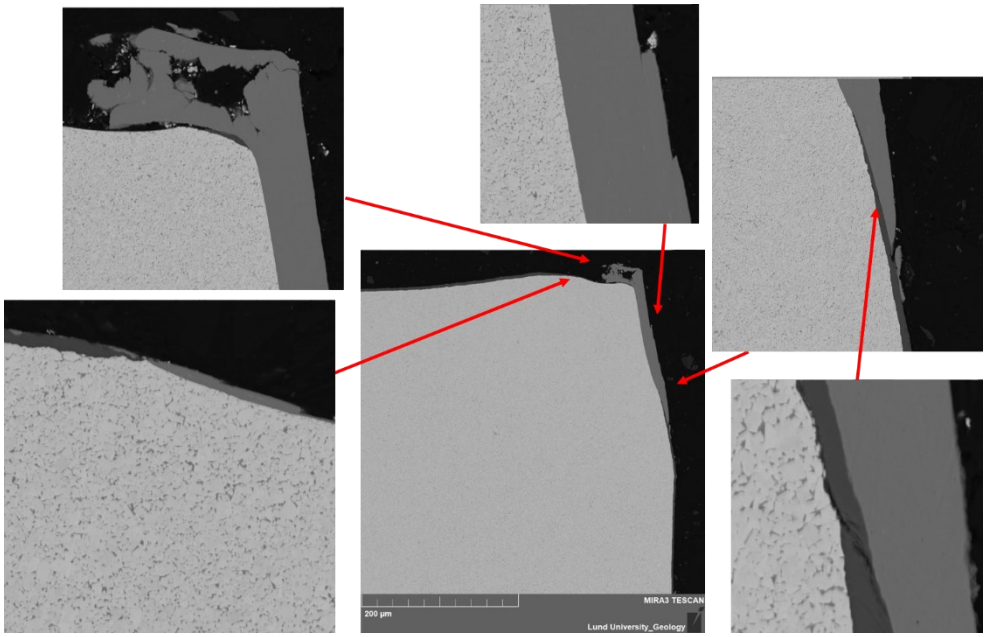

Figure 4-18 Cross section of TiN, machined 5 seconds in argon at v_c = 200 m/min.

Figure 4-19 and Figure 4-20 show example of EDX scan results from the rake side (these images being twisted 90 º) from areas of adhered material (Ni, Cr, Fe and Nb) on the coating. As mentioned above, O Kα peak and Cr Lα peak are close to each other in the EDX spectrum, when the signals are weak these two are being questioned whether these are interfering each other.

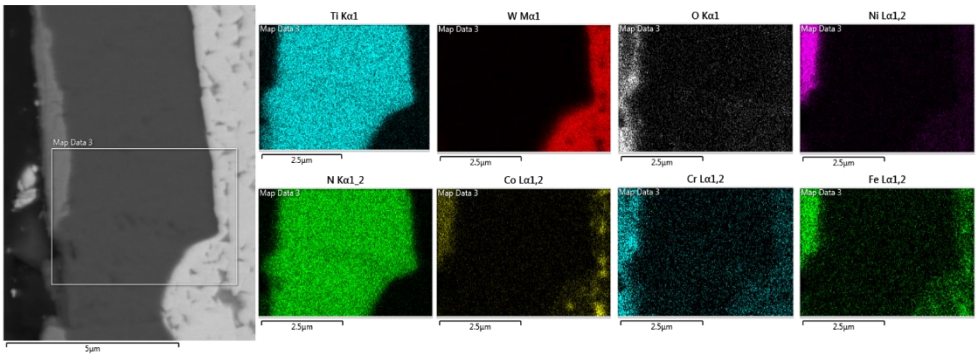

Figure 4-19 EDX of TiN cross section, machined 5 seconds in HP air at v_c = 200 m/min.

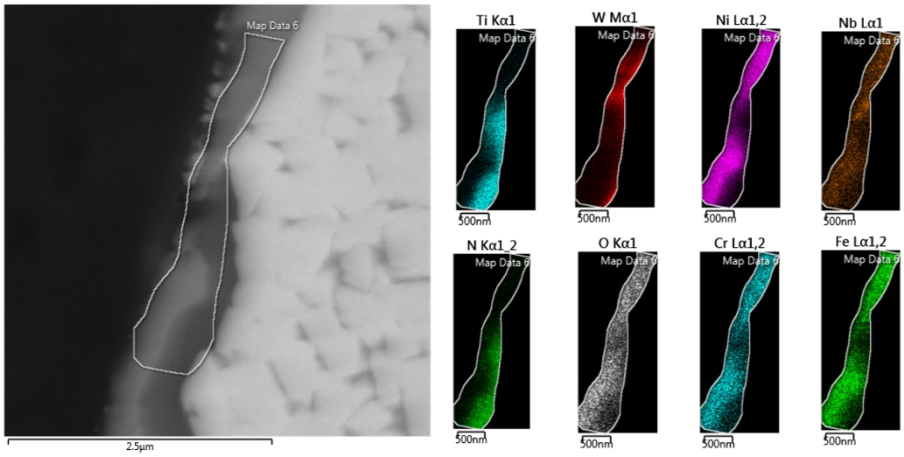

Figure 4-20 EDX of TiN cross section, machined 5 seconds in argon at v_c = 200 m/min.

4.3.1.2. TiAlN

Figure 4-21 and Figure 4-22 shows the rake face of the TiAlN coating which appears intact. The tool-chip contact is clearly visible, as shown in Figure 4-11, and some debris outside it. It appears to be some adhered material on the edge line of both tools, which in general performs similar.

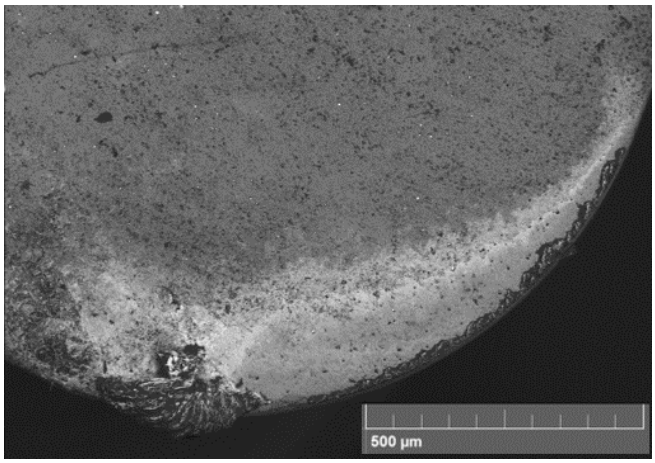

Figure 4-21 Back-scattered image of TiAlN surface, machined 5 seconds in HP air at v_c = 200 m/min.

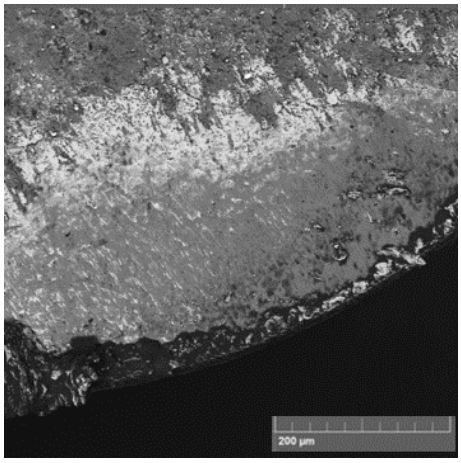

Figure 4-22 Back-scattered image of TiAlN surface, machined 5 seconds in argon at v_c = 200 m/min.

The surface of the TiAlN coating, Figure 4-23 and Figure 4-24, show similar result for the air and argon environment, but there is slightly more adhered material when machining in argon. The coating appears intact, though shadowed by adhered material (Ni, Nb, Cr and Fe) still found after the etching process. The signals are noisy partly due to the adhered material and possibly due to a big scanning distance on the tool machined in HP air. Cr and O does not appear to impact each other as much in these two scans. The scanned line is chosen with the knowledge that there is more oxygen available in the area just outside the tool-chip contact area, with it being more likely to find oxides. With the amount of adhered material, there are no conclusions drawn to a possible oxidized coating, with it possibly being the adhered material that is oxidized on top of the coating.

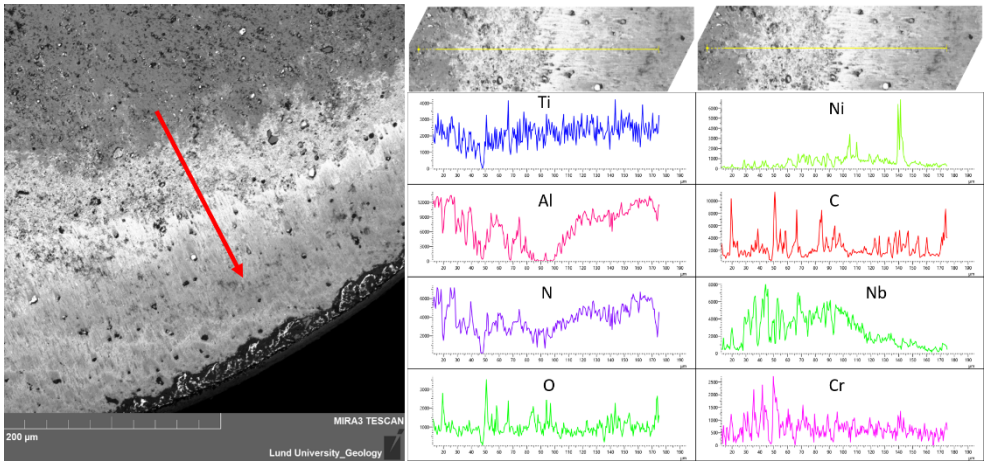

Figure 4-23 Surface EDX of TiAlN, machined 5 seconds in HP air at v_c = 200 m/min.

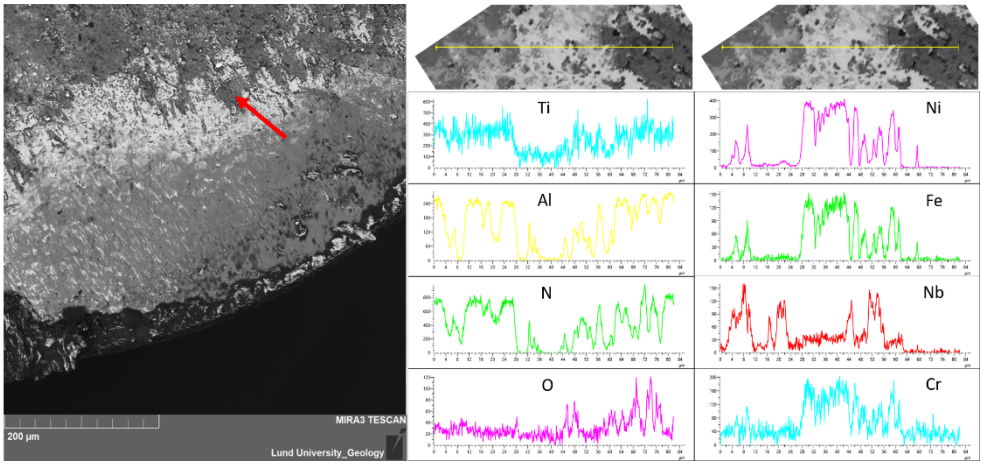

Figure 4-24 Surface EDX of TiAlN, machined 5 seconds in argon at v_c = 200 m/min.

The SEM images, Figure 4-25 and Figure 4-26, show that the coating is more or less intact and with some adhered material. Some cracks and weak points can be seen, and the coating integrity is maintained and no sign of plastic deformation of the tools was seen. Both from the HP air- and argon tools, strings were found (upper right image in Figure 4-25 and lower left in Figure 4-26) which appears to be binder material from the substrate. Droplets with higher concentration of Ti were found in several places.

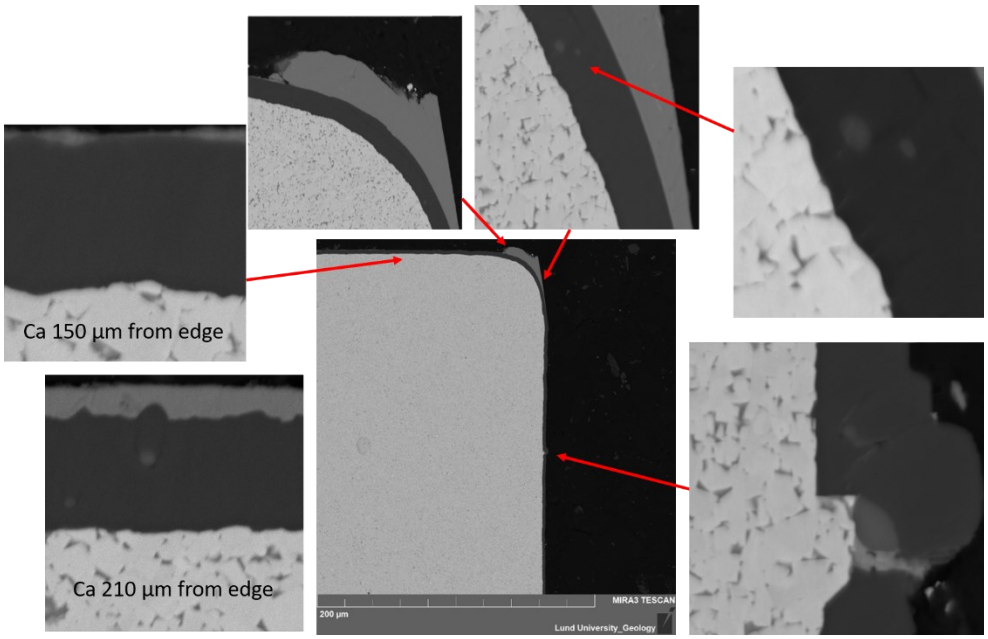

Figure 4-25 Cross section of TiAlN, machined 5 seconds in HP air at v_c = 200 m/min.

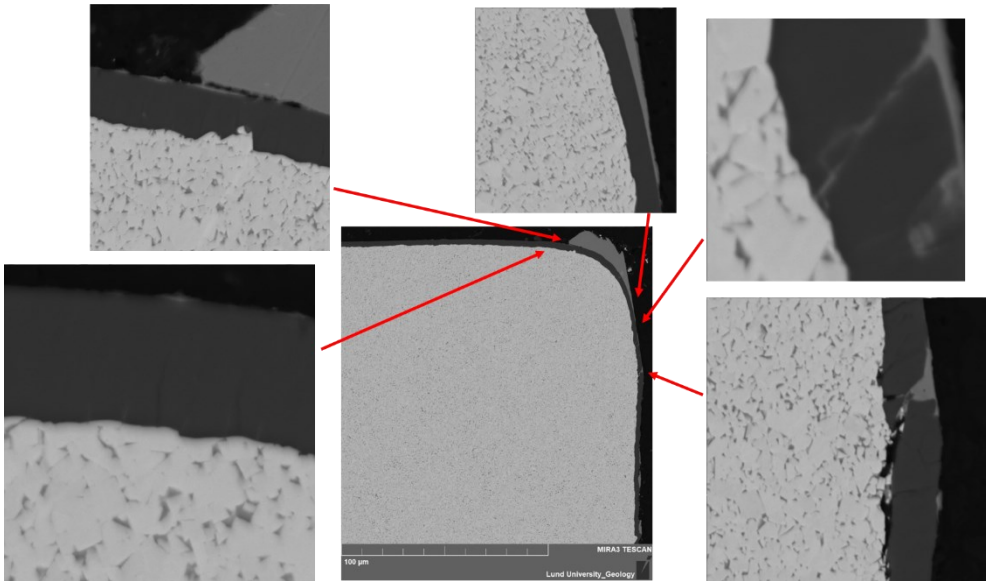

Figure 4-26 Cross section of TiAlN, machined 5 seconds in argon at v_c = 200 m/min.

Examples of EDX results, Figure 4-27 and Figure 4-28, show that there are no obvious reactions between the coating and the adhered material. These images were taken on the rake side about 210 µm and 170 µm from the edge, respectively, which was chosen since this is in the sliding zone, where the possibility of oxygen is higher. However, no signs of oxidation was found on any scans in these regions. Figure 4-27 show one example of the droplets mentioned earlier consisting of Ti.

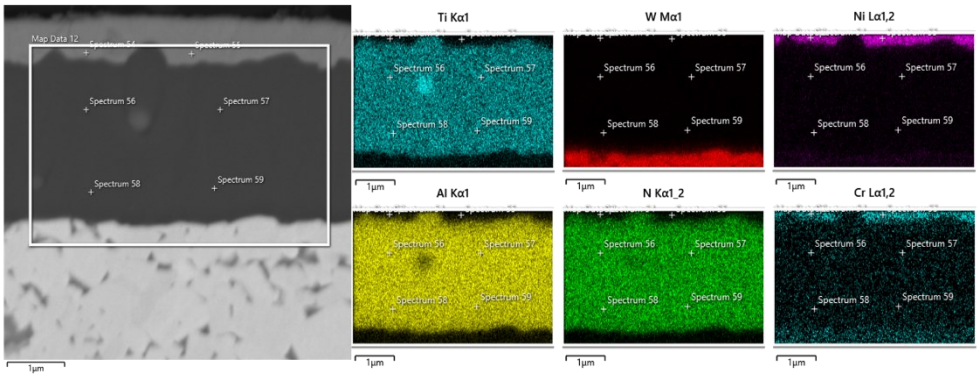

Figure 4-27 EDX of TiAlN cross section, machined 5 seconds in HP air at v_c = 200 m/min.

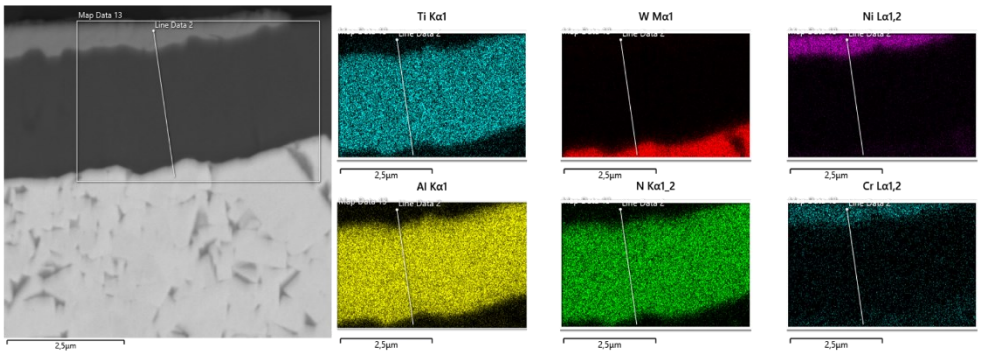

Figure 4-28 EDX of TiAlN cross section, machined 5 seconds in argon at v_c = 200 m/min.

4.3.1.3. C3

The two runs of C3, Figure 4-29 and Figure 4-30, shows quite similar result for both environments, the adhered material on the edge line appears relatively high. Both tools appear intact on the rake face. Comparing the debris and adhered material outside the contact zone with the TiAlN, the C3 appears to have more of it.

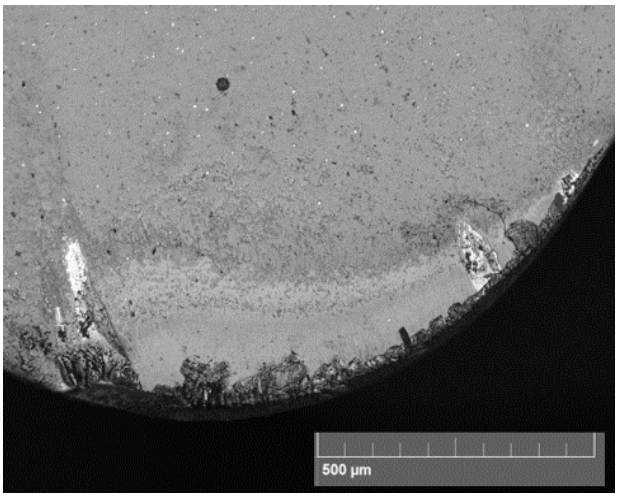

Figure 4-29 Back-scattered image of C3 surface, machined 5 seconds in HP air at v_c = 200 m/min.

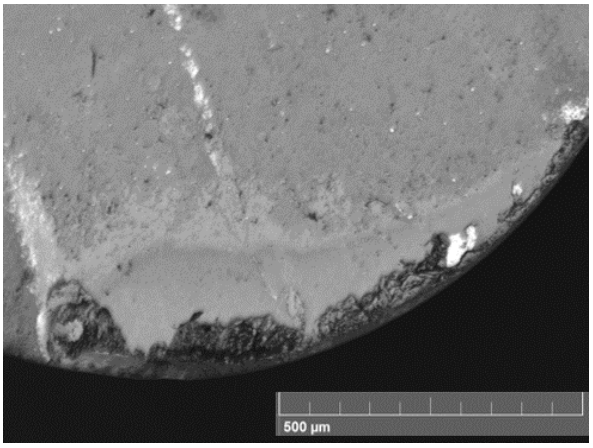

Figure 4-30 Back-scattered image of C3 surface, machined 5 seconds in argon at v_c = 200 m/min.

Flank wear is noticed on both tools from SEM images on the cross section, Figure 4-31 and Figure 4-32, with coating gone on parts of the flank. The tool that was run in the air environment has a distinct crater without any coating left and both tools show signs of plastic deformation. On the tool that were run in argon, the coating appears to be intact on the rake. Droplets from the deposition of this coating appears to be relatively high.

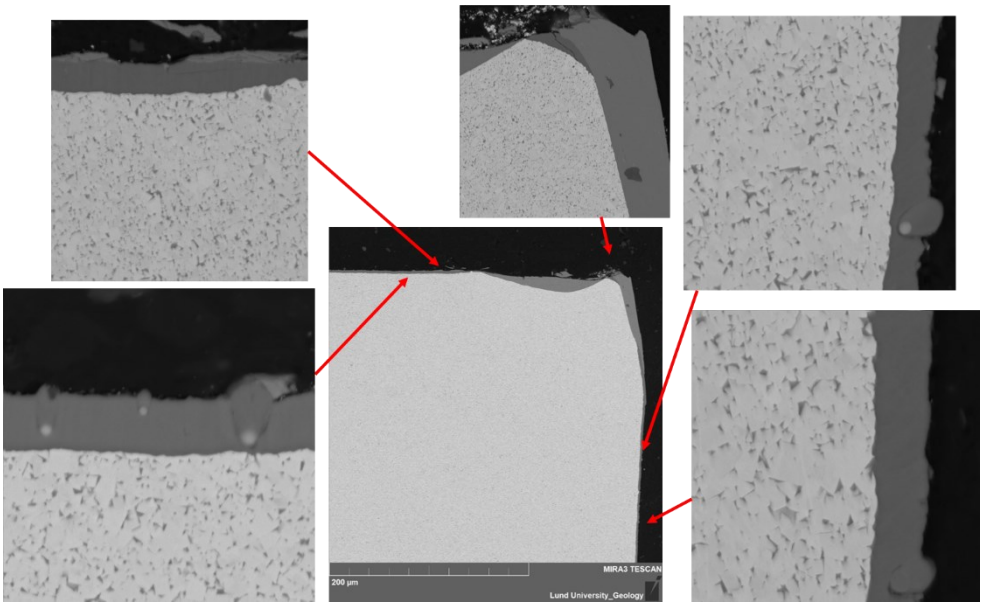

Figure 4-31 Cross section of C3, machined 5 seconds in HP air at v_c = 200 m/min.

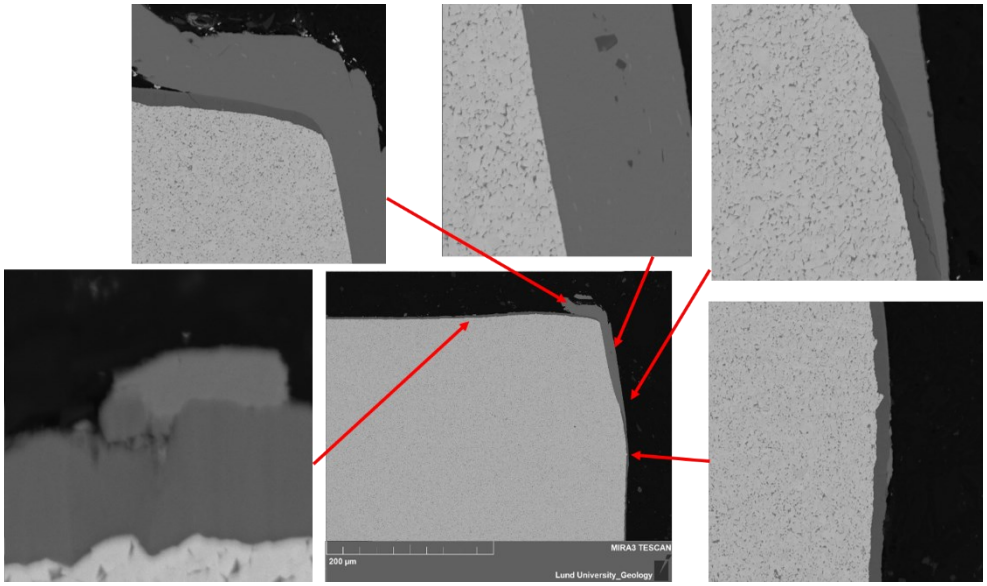

Figure 4-32 Cross section of C3, machined 5 seconds in argon at v_c = 200 m/min.

4.3.1.4. C4

Figure 4-33 and Figure 4-34 show that the coating is intact on the rake face in both cases, with it being slightly less adhered material on the edge line compared to C3. Like the C3, there are quite a lot of adhered material and debris outside the contact zone.

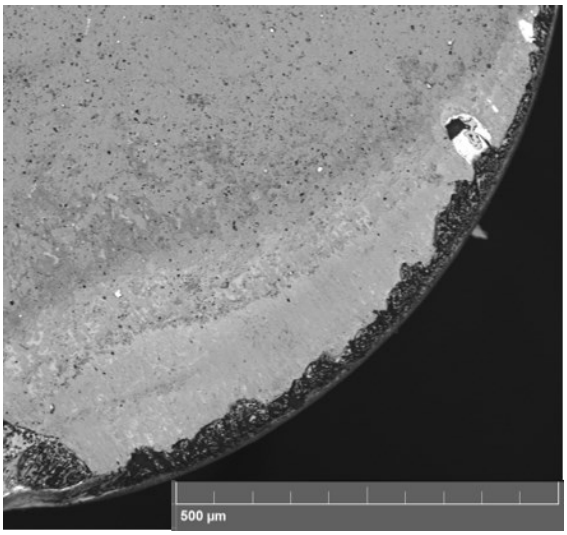

Figure 4-33 Back-scattered image of C4 surface, machined 5 seconds in HP air at v_c = 200 m/min.

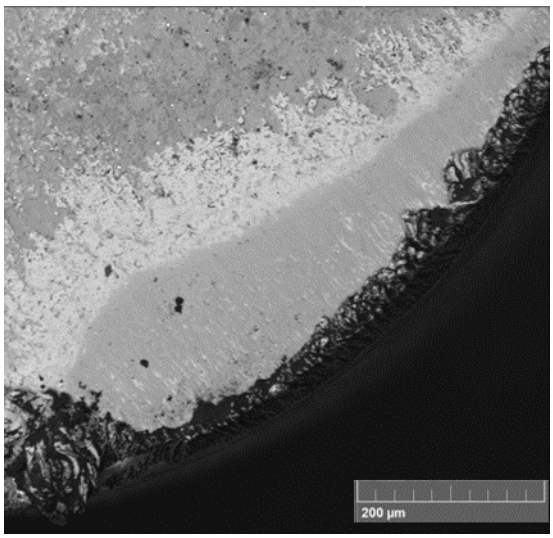

Figure 4-34 Back-scattered image of C4 surface, machined 5 seconds in argon at v_c = 200 m/min.

The cross sections of the C4 coating, Figure 4-35 and Figure 4-36, shows some flank wear where the coating is worn away, similar to the C3 result, but not as big flank wear. In the lower left of Figure 4-36, there is a probable defect from where a droplet have been torn away and left a grove, which is filled with adhered material. Strings with binder material from the substrate are found, both in the upper left part of Figure 4-35 and the top right of Figure 4-36, similar to the findings in the TiAlN coating.

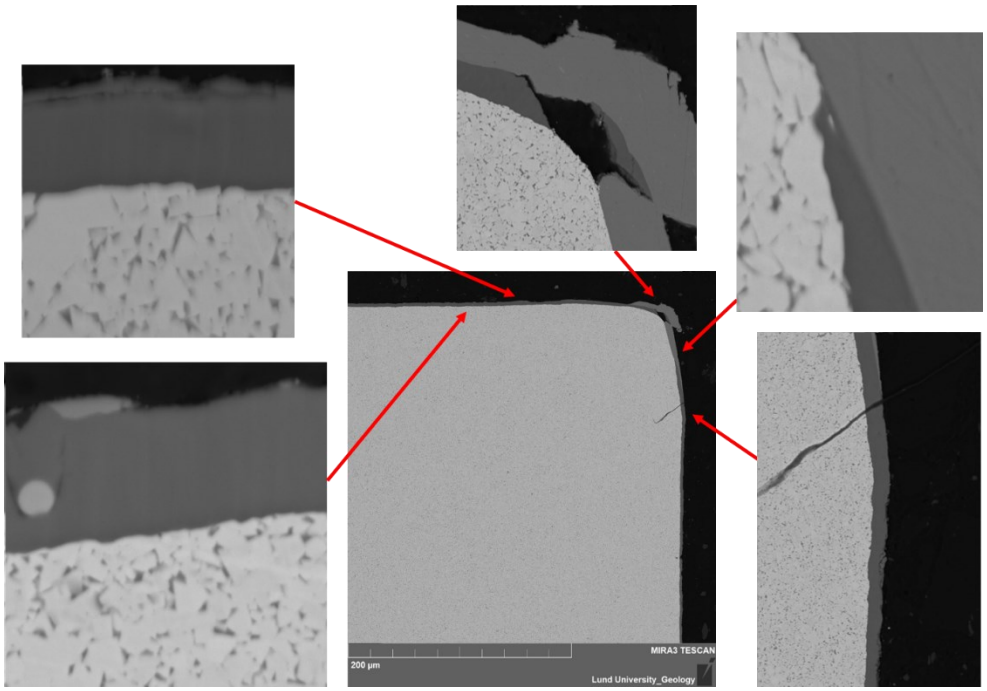

Figure 4-35 Cross section of C4, machined 5 seconds in HP air at v_c = 200 m/min.

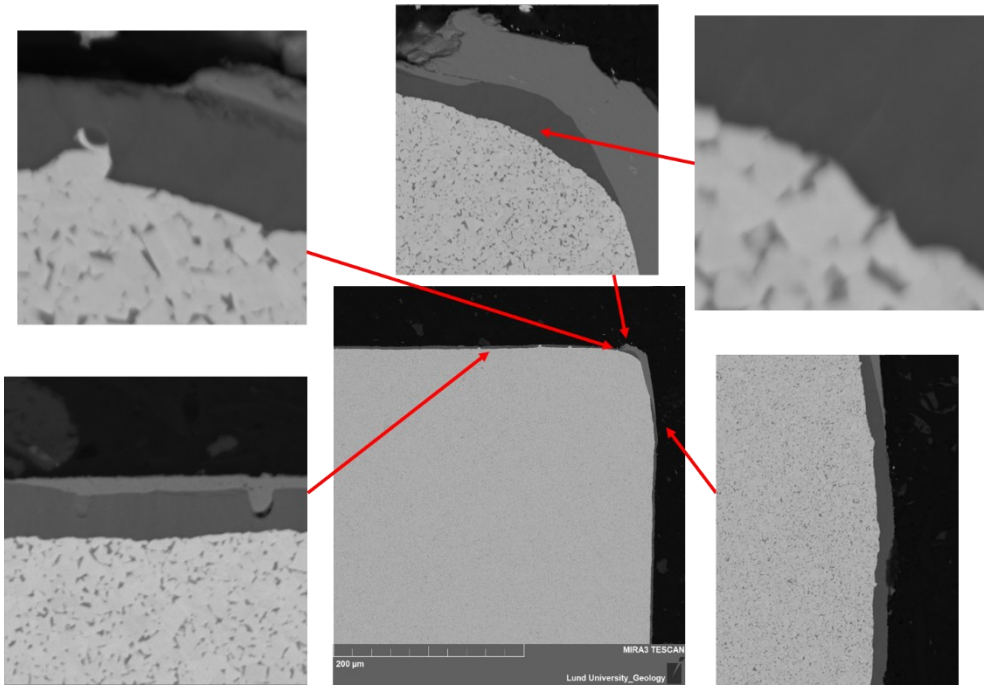

Figure 4-36 Cross section of C4, machined 5 seconds in argon at v_c = 200 m/min.

4.3.2. Performance test

This section presents results of TiN, TiAlN, C3 and C4 from machining tests that used the cutting conditions stated in Table 3-3. Individual results are first presented and compared in the end of this chapter.

4.3.2.1. TiN

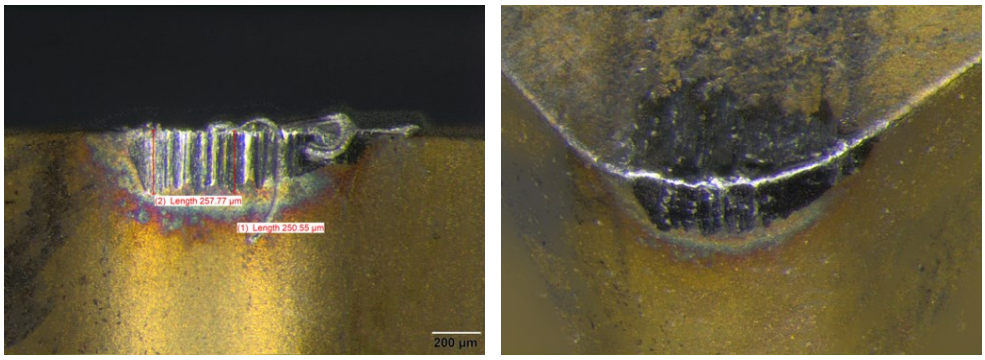

Figure 4-37 TiN flank (left) and flank+rake (right), machined at 60 m/min for 1.5 min in HP air.

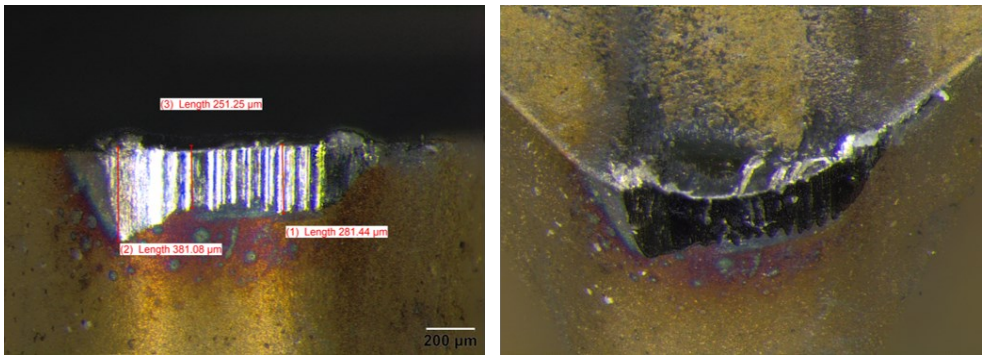

Figure 4-38 TiN flank (left) and flank+rake (right), machined at 60 m/min for 1.5 min in argon.

TiN machined in HP air performs better in general compared to argon environment. Maximum flank wear limit of 200 µm was exceeded after 1.5 min, and the measured results are presented in Table 4-1.

Table 4-1 TiN performance test results, machined at 60 m/min for 1,5 min.

VB,max		
Ar (µm)	**HP air (µm)**	**Argon performance compared to air**
281	251	-11 %
Notch		
Ar (µm)	**HP air (µm)**	**Argon performance compared to air**
381	258	-47 %

4.3.2.2. TiAlN

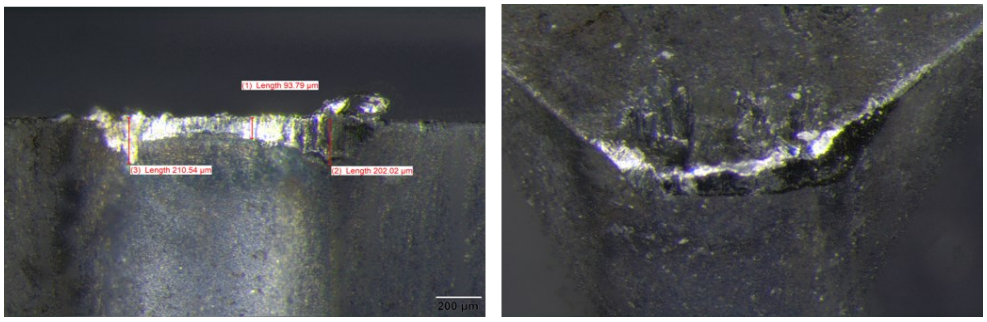

Figure 4-39 TiAlN flank (after 5 min, left) and flank+rake (after 7 min, right), machined at 60 m/min in HP air.

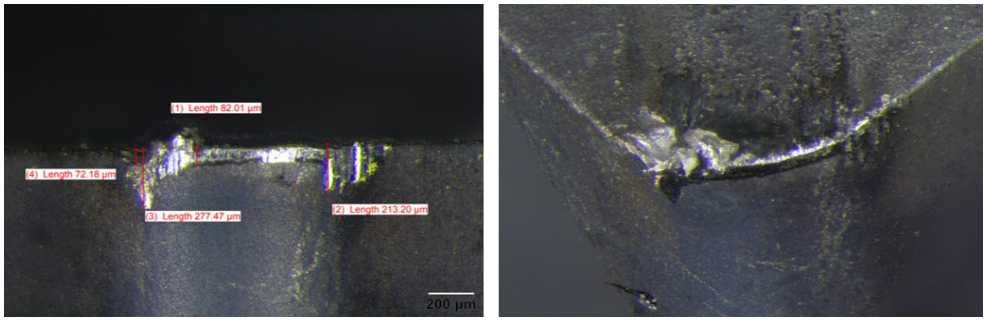

Figure 4-40 TiAlN flank (left) and flank+rake (right), machined at 60 m/min for 5 min in argon.

The overview image of the rake and flank side (to the right in Figure 4-39) of TiAlN machined in air was taken after 7 minutes of engagement time, which should be considered when comparing with the image of the tool run in argon environment. TiAlN machined in HP air performs better in general compared to argon environment. Maximum flank wear limit of 200 µm was exceeded after 5 min, measured results presented in Table 4-2. Table 4-2 TiAlN performance test results, machined at 60 m/min for 5 min

Table 4-2 TiAlN performance test results, machined at 60 m/min for 5 min.

VB,max		
Ar (µm)	**HP air (µm)**	**Argon performance compared to air**
213	202	-5 %
Notch		
Ar (µm)	**HP air (µm)**	**Argon performance compared to air**
277	211	-31 %

4.3.2.3. C3

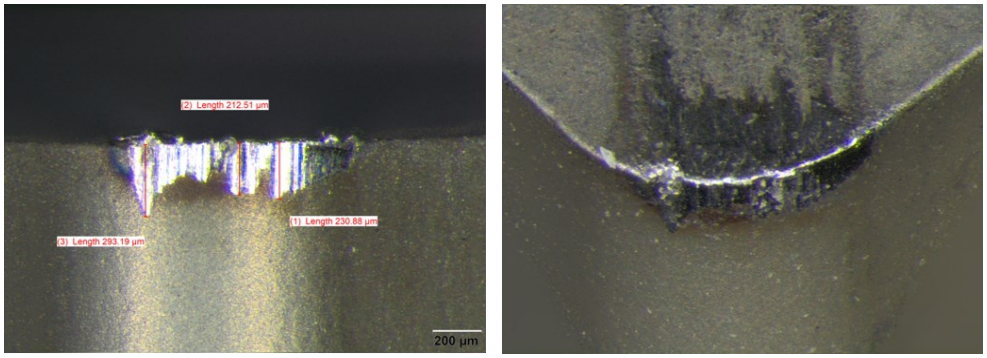

Figure 4-41 C3 flank (left) and flank+rake (right), machined at 60 m/min for 1.5 min in HP air.

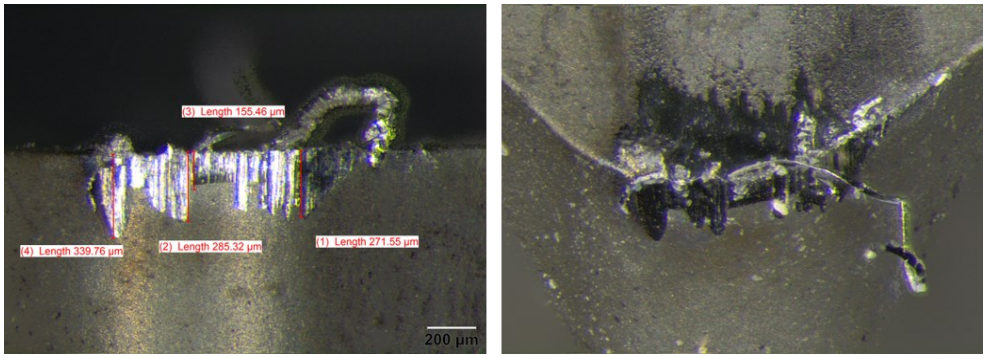

Figure 4-42 C3 flank (left) and flank+rake (right), machined at 60 m/min for 1.5 min in argon.

C3 machined in HP air performs better in general compared to argon environment. Maximum flank wear limit of 200 µm was exceeded after 1.5 min, measured results presented in Table 4-3.

Table 4-3 C3 performance test results, machined at 60 m/min for 1.5 min.

VB,max		
Ar (µm)	**HP air (µm)**	**Argon performance compared to air**
285	231	-23 %
Notch		
Ar (µm)	**HP air (µm)**	**Argon performance compared to air**
349	258	-35 %

4.3.2.4. C4

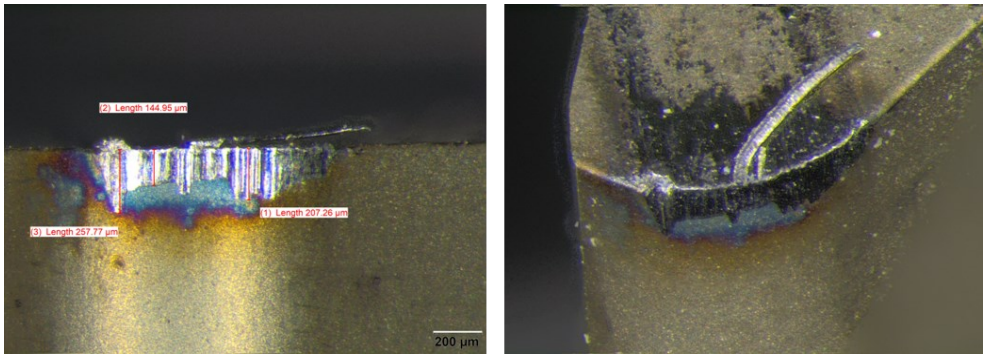

Figure 4-43 C4 flank (left) and flank+rake (right), machined at 60 m/min for 1.5 min in air.

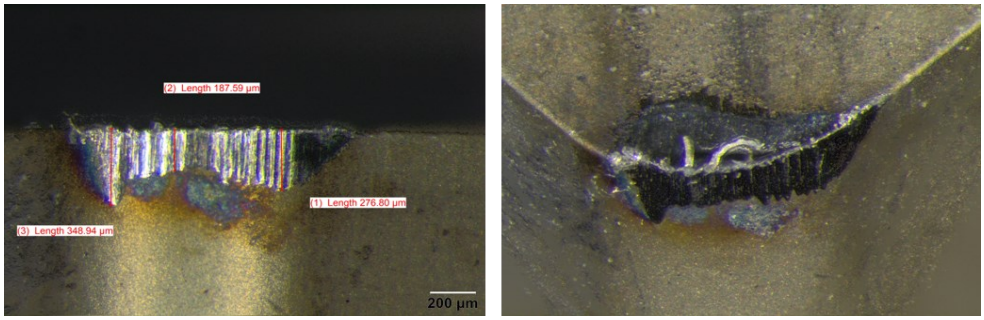

Figure 4-44 C4 flank (left) and flank+rake (right), machined at 60 m/min for 1.5 min in argon.

C4 machined in HP air performs better in general compared to argon environment. Maximum flank wear limit of 200 µm was exceeded after 1.5 min, measured results presented in Table 4-4.

Table 4-4 C4 performance test results, machined at 60 m/min for 1.5 min.

VB,max		
Ar (µm)	**HP air (µm)**	**Argon performance compared to air**
277	207	-33 %
Notch		
Ar (µm)	**HP air (µm)**	**Argon performance compared to air**
340	293	-16 %

Summarized results from the performance test presented in Figure 4-45 and Figure 4-46 below. In average the coatings measured flank wear is 18% bigger when machined in argon environment compared to high pressure air, notch is measured to be 33% bigger in average.

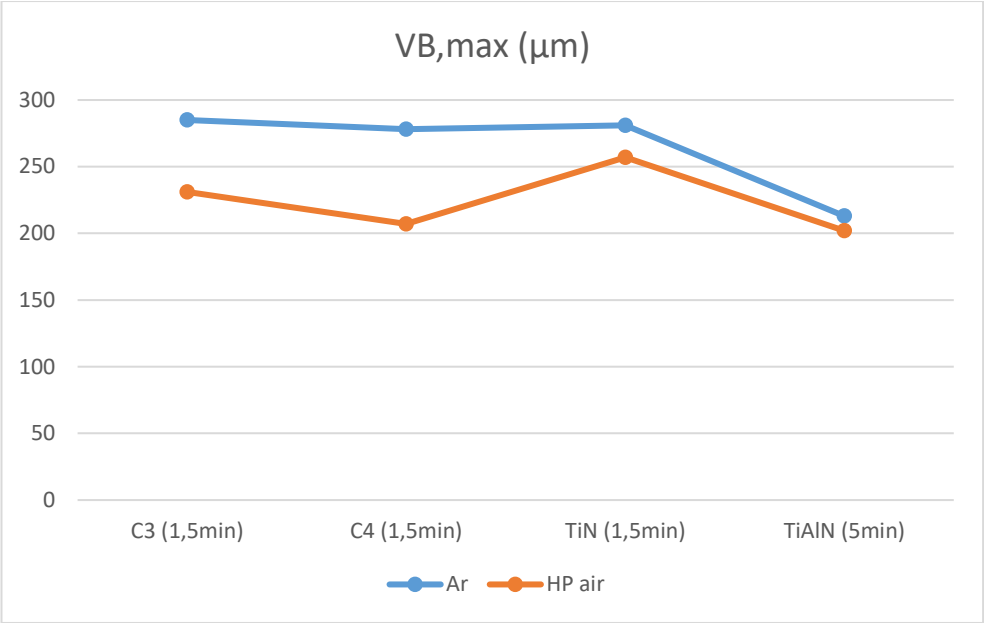

Figure 4-45 Maximum flank wear measured from performance test of C3, C4, TiN and TiAlN coatings, in argon- respectively high pressure air environment.

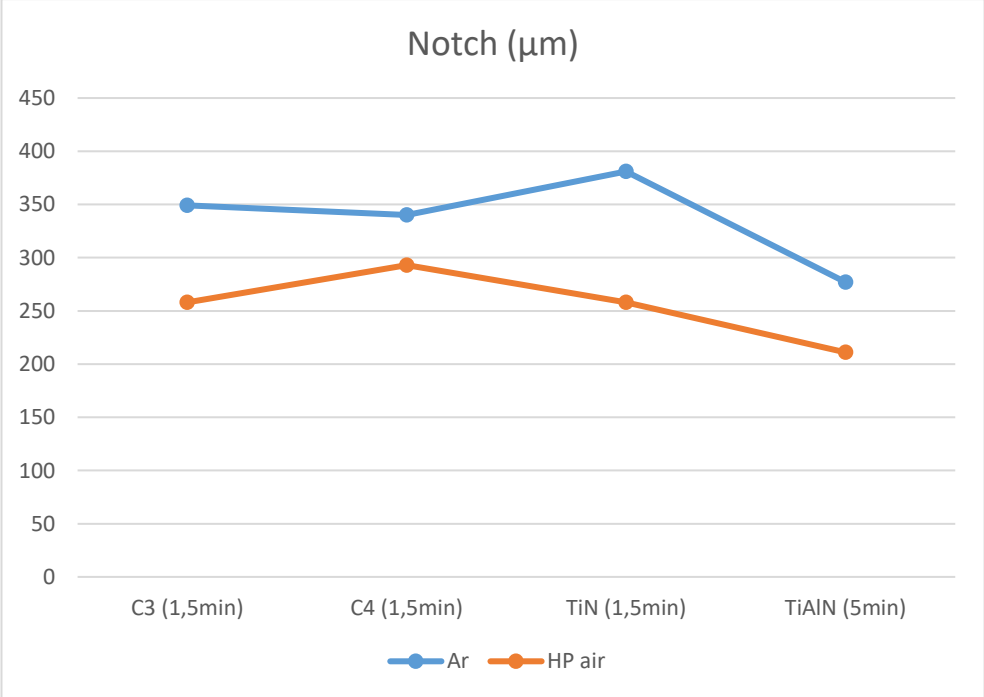

Figure 4-46 Notch measured from performance test of C3, C4, TiN and TiAlN coatings, in argon- respectively high pressure air environment.

4.3.3. C4 short time test

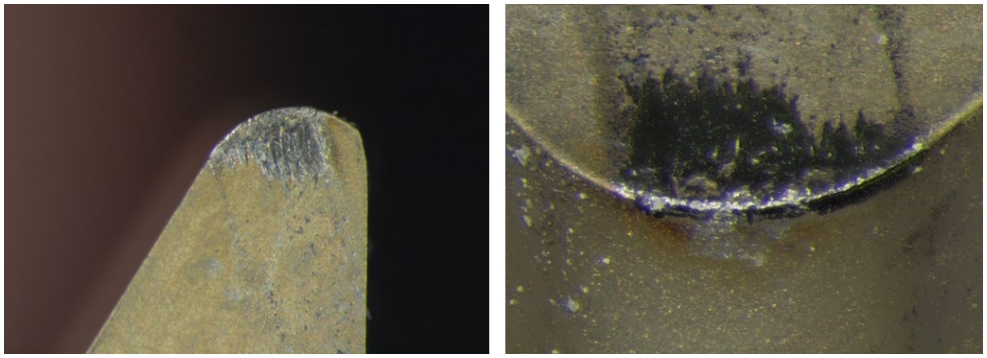

Figure 4-47 C4 coating machined at 60 m/min for 10 seconds in HP air, cut tools rake (left) and overview (right).

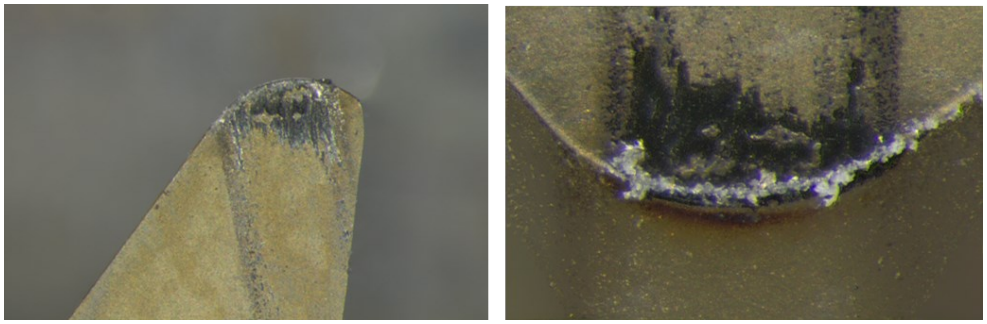

Figure 4-48 C4 coating machined at 60 m/min for 20 seconds in HP air, cut tools rake (left) and overview (right).

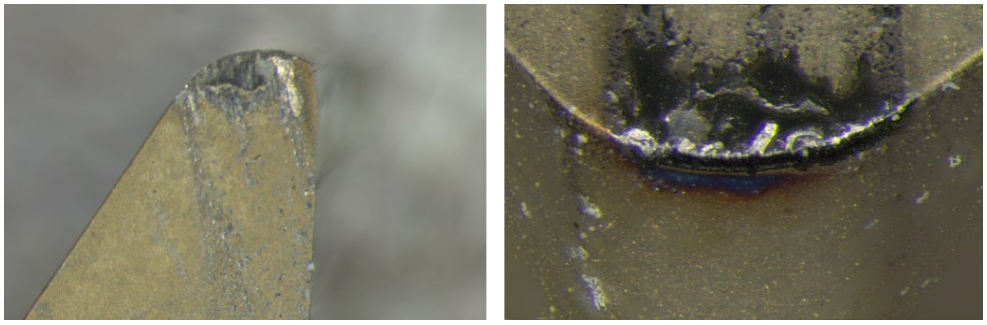

Figure 4-49 C4 coating machined at 60 m/min for 30 seconds in HP air, cut tools rake (left) and overview (right).

Images, Figure 4-47 to Figure 4-49, from the optical microscope with three tools being machined for 10, 20 and 30 seconds respectively. Below back scattered electron images of cross section from each tool are presented.

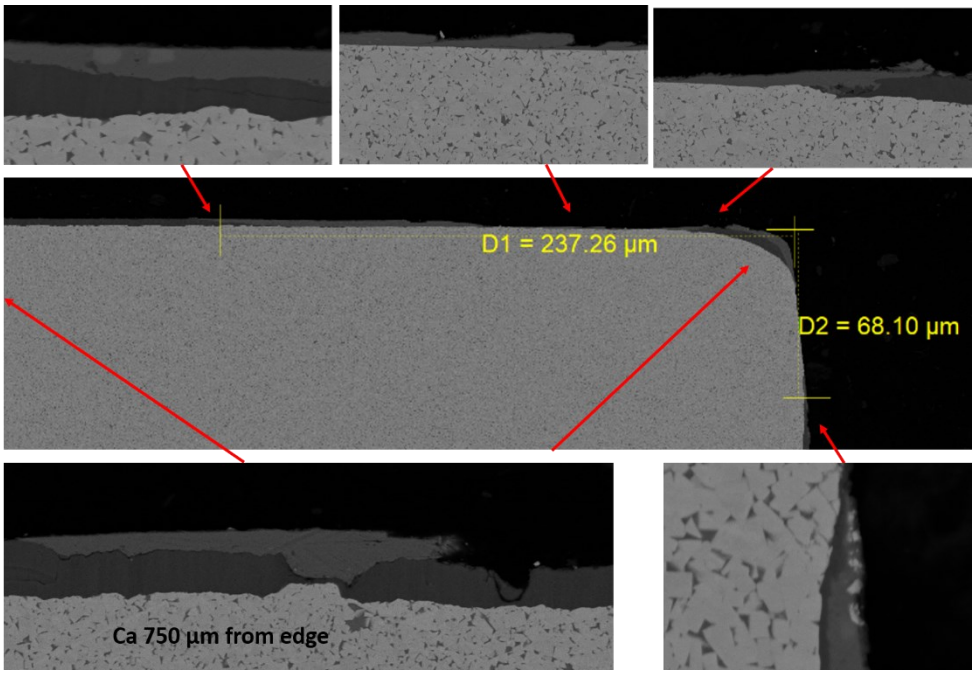

Figure 4-50 Back scattered electron image of cross section of C4, machined for 10 seconds.

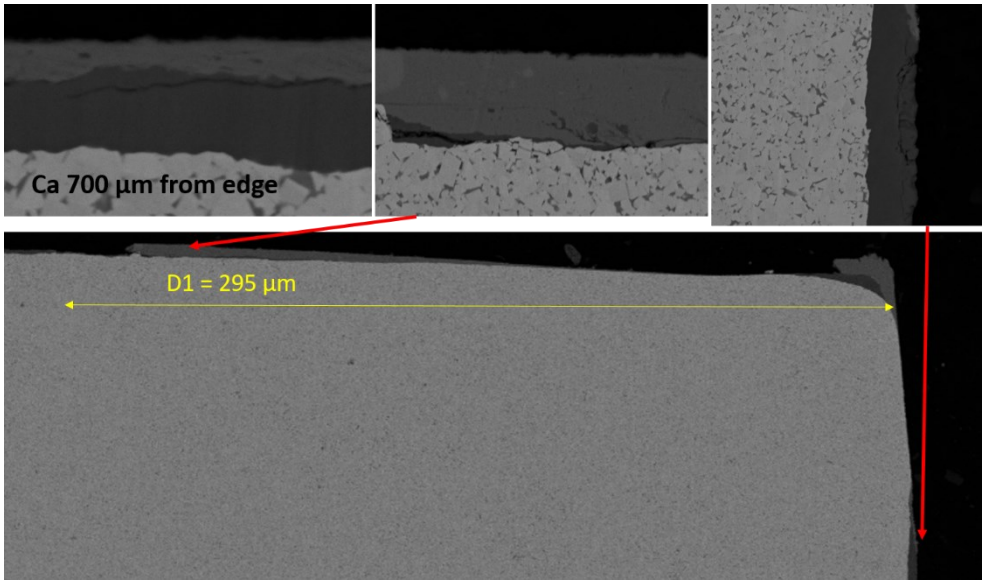

Figure 4-51 Back scattered electron image of cross section of C4, machined for 20 seconds.

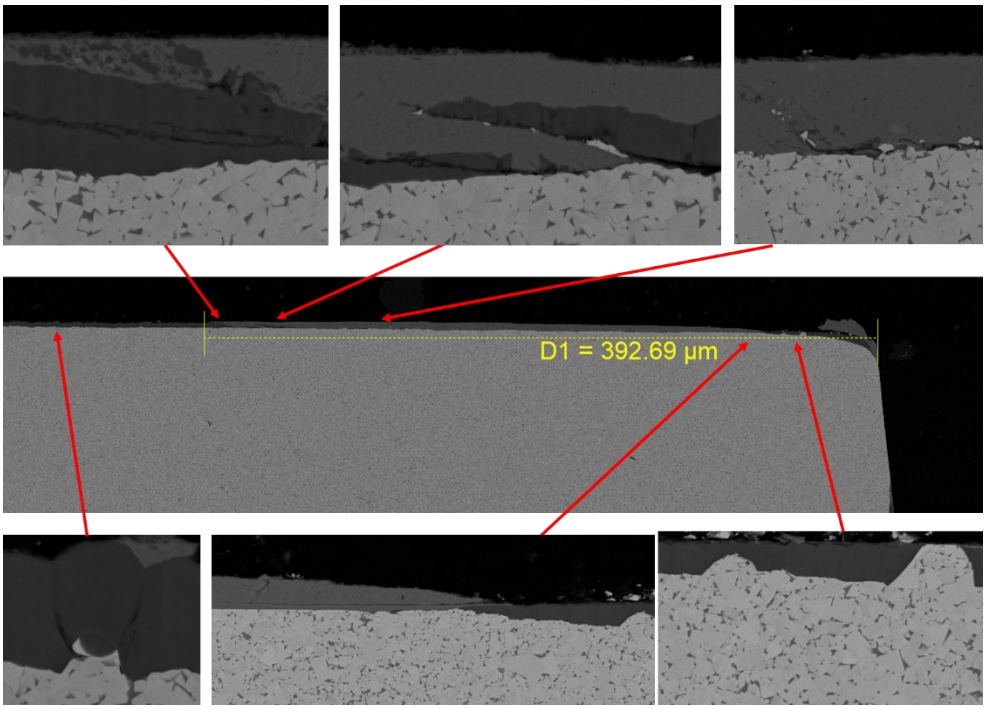

Figure 4-52 Back scattered electron image of cross section of C4, machined for 30 seconds.

The distance from the edge to the place on the rake where the coating seems to have original coating thickness was measured. For the tool machined for 10 seconds it was measured to 237 µm, the 20 seconds tool was measured to 295 µm and the 30 seconds tool was measured to 393 µm. In the upper middle part of Figure 4-52 a part of the coating appears to just have been torn away from the substrate and would probably follow the flow of the chips.

5. Discussion

In this chapter, the results from furnace and machining experiments are discussed.

5.1. Furnace test

From the furnace test, there is a clear difference of the oxidation resistance between the tested coatings. TiAlN has barely started to oxidize, which is somewhat expected since other studies, mentioned in section 2.1.4.2, shows that 800 °C is the temperature where this coating just starts to oxidize with a maximum oxidation growth at around 950 °C. As a comparison the TiN starts to oxidize at 500 °C and at maximum rate at 750 °C. With the planned Thermogravimetric analysis this mapping was supposed to be performed for all six coatings to understand the oxidation tendency and critical temperatures better.

It appears that the C3 coating creates more of a protective and denser oxide scale compared to the C4 coating. The oxide scale on the C4 coating is about five times as thick compared to the C3, which is a clear difference in oxidation resistance and the C3 coating is performing better than C4 in this test. If there is a higher tendency of droplets from the deposition process, as seen in Figure 4-31 which C3 appears to have more of compared to the other coatings, with somewhat of a pocket around the droplet where oxygen can travel, this should be considered as a weak point not to disregard.

The TiN coating gets about twice as thick when oxidized, Figure 4-5, and the coating is almost fully oxidized and appears porous. This is somewhat expected since the temperature in this test is well over when TiN starts to oxidize, as mentioned above. It is critical for the coating to protect the substrate from oxygen at these high temperatures, which can otherwise lead to a quick growth of the substrate material oxides, which was found in TiN cross section, Figure 4-6.

5.2. Machining

5.2.1. Elevated speed

The C1 and C2 were part of the test, but the results were tool failure at every test (2 runs in HP air and 2 runs in argon environment) of respective coating, these were not analysed further. So, the coatings discussed in this section are C3, C4, TiN and TiAlN.

The comparison of the coating performance at elevated speed was complicated, since it was hard to compare and analyse the results only from the top surface point of view. The etching process was not 100 % successful in removing adhered material,

which made it a bit hard to understand the EDX data. It was still possible to conclude that the TiN performed the worst since the coating was torn away on big parts of the contact zone. C3 and C4 coating both performed better than TiN, with the C4 performing slightly better than the C3. It appears that there is slightly more material and debris adhered on these two concept coatings compared to the TiAlN, which in general performs better than C3 and C4.

Many SEM images were collected and EDX scans were performed, from the rake face it was difficult to draw conclusions due to uncertainties in coherent etching between the tools. With the etching process not as successful as expected there was still adhered material shadowing the surface of the coating, which was the objective to look at. With low amount of a material, the energy peaks got weak and was sometimes suspected to interfere others, like Cr and O, Fe and Co. The thought was that it would be enough to look at the surface of the rake face to find answers of what is forming, which was not possible. The second batch of tools were then decided to be cut to study the cross section, in the middle of the contact zone of the tools. This allowed visualization of the distribution of the oxidation depth of the coating and other related wear mechanisms.

A lot of time were put into preparing the tools to be able to study the cross sectioned tools, described in 3.2.5, which paid off when a more complete picture of the wear of the coatings was collected. About 290 EDX reports have been exported and analysed from the tools used in the elevated conditions, and a few of the results have been included in this report.

No clear signs of diffusion or chemical interaction between the coating- and workpiece material were found. This was not expected and caused some confusion whether there was something done wrong or not working properly. There was adhered material on many places and tool-/environment combination, but at the few places where oxides were found, it appeared to be the workpiece material that was oxidized and adhered on the coating. It seems that the coatings did not wear through oxidation, but rather mechanically or tribologically, and that conditions when the coatings oxidize were never reached in these tests.

5.2.2. Performance test

The high speed machining test discussed in the previous section was designed to reach possible oxidation temperatures. In the performance test, the cutting speed was much lower (60 m/min), which should result in much lower temperatures.

The TiAlN was performing a lot better than TiN, C3 and C4. TiAlN was expected to perform well, but that it took more than 3 times as long to reach the wear limit was surprising.

TiN, C3 and C4 all exceeded the wear limit after 1.5 min and when comparing the maximum flank wear, the C4 performs the best, only slightly better in argon environment. When comparing notch wear, the C4 is not as strong, but the result does not differ as much depending on the environment as the C3 and TiN does. In general, the wear is bigger when machining in the argon environment, which previous research also concludes.

It is concluded that there is a great difference between the coatings, with the TiAlN performing a lot better in the lower speed test as well. The oxidation resistance should not play a big role since the temperatures reached are lower than in the high-speed test. This, again, confirms the hypothesis above, that the mechanical and tribological strength of TiAlN has the biggest impact of the coating's performance when machining Alloy 718 material.

5.2.3. C4 short time test

The expectations of this additional test were that we would see a small difference since these tools were tested for such short time, and maybe that we would not see anything after only 10 seconds. This test turned out to give surprisingly value-adding information of the coating degradation mechanism.

The tool machined for 10 seconds had about 240 µm of clean substrate material on the rake face, which was surprising. The tool in general does not appear to be in a bad condition, but the coating is clearly mechanically worn away and parts of the coating was found in the adhered material transporting the coating away with the chips. This was most clearly found in the images of the 30 seconds tool, Figure 4-52. In general, the coating appeared to be torn away in very small pieces, but in this mentioned case, there was a bigger part of the coating found in the adhered material torn from the substrate.

This last machining experiment answered the unexpected results of this project and why there were barely any oxidation found. Instead, the TiN, C3 and C4 coatings are mechanically removed by an adhesive wear mechanism caused by the strong adhesive effect between the coating and the workpiece material.

6. Conclusions

There are differences in the oxidation resistance of the tested coatings when subjecting the tools to a thermal exposure environment. At 800 ºC in air atmosphere in a furnace, the C3 coating creates a protective and dense oxide scale, C4 forms an oxide scale three times thicker than C3 and appears more porous. The TiN oxidizes all the way through the coating, which grows to twice the thickness. TiAlN does not oxidize at this temperature and is considered to perform the best, C3 second best followed by C4, and the TiN showed the poorest performance at these conditions.

There were barely any signs of oxidation from the High speed cutting test, with cutting conditions on the very edge of surviving after 5 seconds. The TiAlN was not worn, the two concepts (C3 and C4) that survived, are worn, and the TiN was in worse shape than the concepts. Some differences in results are noticed for the two different environments, though it does not seem to be connected to oxidation, and rather being connected to different adhesive effect in different environments. It was important to have a look at the cross section to get a complete picture of the result. The major conclusion from this test is that TiAlN is considerably stronger than the rest of the coatings, but that it is probably not connected to oxidation resistance.

The Performance test also showed that the TiAlN is performing a lot better than the rest of the coatings. C3, C4 and TiN are performing similar and are not close to the performance of the TiAlN. This test was done at lower cutting speed (and temperature), which suggests that there are other performance factors, rather than oxidation resistance, which makes the TiAlN coating performing well when machining Alloy 718. Looking at the cross section of C4 coating after machining 10, 20, and 30 seconds, respectively, we see that the workpiece material adheres strongly to the coating, and is mechanically worn and fails to protect the substrate material.

Overall, C4 performs slightly better than C3 when machining and the opposite in the Furnace test, and that both perform better than TiN in both tests. TiAlN barely reaches its potential when using conditions used, not to exceed the limits of C3, C4 and TiN coatings. Droplets from the depositioning seem to weaken the integrity of the coating and has been found when looking at the cross section of all coatings, and it is shown that they can have big impact on the result if they are in the wrong place.

This means that, as these experiments has been designed, oxidation resistance appears to play a marginal, or no role, when comparing the chosen concept coatings performance to TiN and TiAlN during continuous cutting of Alloy 718. It rather appears that the mechanical wear resistance and the ability of workpiece material to strongly adhere to the coating is differing and has a big impact of the wear resistance of the coatings.

7. Future work

Something that was discussed when planning which concept coatings should be tested, adding aluminium in the concept mixes is something that would be interesting. To see, for example, if the hardening mechanism of the Al in the TiAlN coating can add value to the performance of other coatings as well. This would be interesting to do, to possibly strengthen the concept coatings and see a potential positive change in the performance.

With the powder of the coating being prepared but unfortunately not tested, would be interesting to finish to get a better understanding of the oxidation resistance and its variation between the coatings. The result of this report would probably not have changed with this result, but it would give a more complete picture of temperature dependent oxidation rates.

Testing of these coatings with different workpiece material would give a better understanding of the coatings potential. The experiments in this study are somewhat narrow and can be widened, though it should not be underestimated how time consuming it is to widen and make changes in the setup and cutting conditions.

There are many tests and articles about the TiAlN coating and its high performance. In this study, its full potential has not been tested, with the weaker coatings holding the cutting conditions and procedure at an easy level for the TiAlN.

References

[1] J.-E. Ståhl, Metal Cutting Theories and Models, Lund, Sweden: SECO TOOLS, 2012.

[2] J.-E. Ståhl, Writer, *Metal cutting - Advanced Course (lecture).* [Performance]. Division of Industrial Produciton, Production and Materials Engineering, Faculty of Engineering, Lunds University, 2018.

[3] "ISO 3685 - Tool-life testing with singel-point turning tools," ISO (the International Organization for Standardization), Second edition, 1993.

[4] J. William D. Callister, Materials science and engineering : an introduction - 7th edition, ISBN-13: 978-0-471-73696-7, Salt Lake City, USA: Jon Wiley and Sons, Inc., 2007.

[5] V. Bushlya, F. Lenrick, J.-E. Ståhl and R. M'Saoubi, "Influence of oxygen on the tool wear in machining," *CIRP Annals - Manufacturing Technology,* no. 67, pp. 79-82, 2018.

[6] G. Greczynski, L. Hultman and M. Odén, "X-ray photoelectron spectroscopy studies of Ti1-xAlxN ($0 \leq x \leq 0.83$) hightemperature oxidation: The crucial role of Al concentration," *Surface and Coating Technology,* no. 374, pp. 923-934, 2019.

[7] J. Chen, "Oxidation behaviour of (Ti,Al)N PVD coatings," Högskolan Dalarna, Falun, 1997.

[8] R. M'Saoubi, M. Johansson and J. Andersson, "Wear mechanisms of PVD-coated PCBN cutting tools," *Wear,* vol. 302, no. 1-2, pp. 1219-1229, April-May 2013.

[9] E. M. Trent and P. K. Wright, Metal cutting, fourth edition, ISBN 0-7506-7069-X, Butterworth-Heinman, 2000.

[10] R. E. Smallman and A. H. W. Ngan, Physical Metallurgy and Advanced Materials, 7th Edition, Butterworth-Heinemann, 2007.

[11] JEOL USA, Inc, "JEOL Posters and Calendars," [Online]. Available: https://www.jeolusa.com/RESOURCES/JEOL-Posters-Calendars/lc/47251/lcv/s/jeol-eds-periodic-table. [Accessed 11 2020].


LUND
UNIVERSITY


LTH
FACULTY OF
ENGINEERING